Master´s Thesis

Sperm flagellar protein 2 expression in mouse tissues and transfection in mIMCD3 cells

Ulla-Maria Sahinaho

University of Jyväskylä

Department of Biological and Environmental Sciences

Cell and Molecular Biology

21.12.2020

UNIVERSITY OF JYVÄSKYLÄ, Faculty of Mathematics and Science
Department of Biological and Environmental Science
Cell and molecular biology

Ulla-Maria Sahinaho: Sperm flagellar protein 2 expression in mouse tissues and transfection in mIMCD3 cells
MSc thesis: 45 p., 2 appendices (4 p.)
Supervisors: Docent Anu Sironen, professor Jari Ylänne
Reviewers: PhD Mari Lehti, PhD Jonna Nykky
December 2020

Keywords: cilia, intraflagellar transport, knockout mouse, primary ciliary dyskinesia, sperm flagella

Male infertility is an increasing problem in Western countries. Male infertility is associated with ciliary dyskinesias, which are diseases of motile cilia. Research on sperm cell development can elucidate causes behind sperm structural and functional defects. Sperm flagellar protein 2 (*Spef2*) gene is expressed in ciliated tissues, and the mutations in *Spef2* cause male infertility. *Spef2* mutant mice have defective cilia in respiratory tract, males are infertile, and the mice develope postnatally a severe hydrocephalus causing lethality. First aim of this study was to develop a novel antibody against adenylate kinase domain (KAD) of SPEF2 protein. Antigen was produced in E. Coli and purified by affinity chromatography. In Western blot, SPEF2 isoforms were detected in wild-type testis, epididymis, lung and oviduct, and a possible novel isoform was observed in brain. Two SPEF2 isoforms were absent in knockout testis. In tissue staining, SPEF2 localized to late spermatocytes, round spermatids, manchette of elongating spermatids, sperm tail midpiece, Sertoli cells, and tracheal epithelial cilia. Second aim of the study was to create a fluorescent cell line to investigate transport of SPEF2 to the cilium and ciliary localization signals. Three SPEF2-GFP fusion proteins were expressed in separate mIMCD3 cell lines: 5'TE-GFP, KAD-GFP, and 3'TE-GFP, which represent different domains of testis-specific *Spef2* sequence. Each fusion protein was localized to the cilium or cilium-associated structures such as basal body, which indicates that *Spef2* contains multiple ciliary localization signals.

JYVÄSKYLÄN YLIOPISTO, Matemaattis-luonnontieteellinen tiedekunta
Bio- ja ympäristötieteiden laitos
Solu- ja molekyylibiologia

Ulla-Maria Sahinaho:	Sperm flagellar protein 2 expression in mouse tissues and transfection in mIMCD3 cells
Pro gradu –tutkielma	45 s., 2 liitettä (4 s.)
Työn ohjaajat:	Dosentti Anu Sironen, professori Jari Ylänne
Tarkastajat:	FT Mari Lehti, FT Jonna Nykky

Joulukuu 2020

Hakusanat: hiirimalli, siittiö, solunsisäinen kuljetus, värekarvasairaus

Miesten hedelmättömyys on kasvava ongelma länsimaissa. Värekarvasairaudet voivat aiheuttaa miesten hedelmättömyyttä. Siittiöiden kehityksen tutkimus voi valaista syitä siittiöiden rakenteellisten ja toiminnallisten vikojen taustalla. Sperm flagellar protein 2 (*Spef2*) -geeni ilmentyy kudoksissa, joissa on liikkuvia värekarvoja, ja se on välttämätön siittiön hännän kehitykselle ja liikkuvuudelle. *Spef2*-knockout hiirimallin avulla tutkittiin *Spef2*:n toimintaa värekarvoissa ja siittiöissä. Liikkuvien värekarvojen toimintahäiriöt aiheuttavat hiirimallilla kroonisia hengitystieinfektioita, siittiövioista johtuvaa hedelmättömyyttä ja vesipäätä. Tämän tutkimuksen tavoite oli kehittää vasta-aine, joka sitoutuu SPEF2:n adenylaattikinaasidomeeniin (KAD). Antigeeni vasta-ainetta varten tuotettiin E.colissa ja puhdistettiin affiniteettikromatografialla. Western blot-menetelmällä ekspressio havaittiin kiveksessä, lisäkiveksessä, keuhkoissa, munanjohtimessa ja mahdollinen uusi isoformi aivoissa. Kaksi SPEF2-isoformia puuttui poistogeenisten hiirten kiveksistä. Kudosvärjäyksissä SPEF2 lokalisoitui spermatosyytteihin, spermatideihin, spermatidien mansettiin, siittiön häntään, Sertolin soluihin ja henkitorven epiteelisolujen värekarvoihin. Toinen tavoite oli kehittää fluoresoiva solulinja, jolla tutkitaan SPEF2:n kuljetusta värekarvaan. Kolme SPEF2-GFP fuusioproteiinia ilmennettiin eri mIMCD3-solulinjoissa. 5´TE-GFP, KAD-GFP ja 3´TE-GFP vastasivat kivesspesifisen *Spef2*-sekvenssin eri toiminnallisia alueita. Fuusioproteiinien paikantuminen värekarvaan tai siihen liittyviin rakenteisiin, kuten basal bodyyn, viittaa että *Spef2*:lla olisi useita värekarvalokalisaatiosignaaleja.

Table of Contents

Abbreviations

AcTub	Acetylated α-tubulin
ADK	Adenylate kinase domain
bgh	*big giant head*
cKO	Conditional gene knockout
CLS	Ciliary localization signal
CPC1	Central pair complex 1
FACS	Fluorescence-activated cell sorter
GFP	Green fluorescent protein
Gtub	γ-tubulin
IFT	Intraflagellar transport
IFT20	Intraflagellar transport protein 20
IMT	Intramanchette transport
ISTS	Immotile short-tail sperm defect
KAD	Adenylate kinase domain in SPEF2
KO	Knockout
mIMCD3	Mouse inner-medullary collecting duct cells
MMAF	Multiple morphological abnormalities of the sperm flagella
MTOC	Microtubule-organizing center

PCD	Primary ciliary dyskinesia
PKD	Polycystic kidney disease
SPEF2	Sperm flagellar protein 2
WT	Wild-type

1 INTRODUCTION

1.1 Cilia

Cilia are cell surface modifications present on nearly every cell in the body. They are hair-like extensions of the apical plasma membrane (Fliegauf et al. 2007). The cilia contain an axoneme, a microtubule-based internal structure. The axoneme extends from the basal body, a centriole-derived, microtubule-organizing center (MTOC) located in the apical region of a ciliated cell. Microtubules are syntezised from α and β tubulin subunits. Tubulins start polymerizing from γ-tubulin ring located in MTOC. Tubulin subunits are added to growing (+) end of microtubules. Ciliary tubulins are acetylated to inhibit depolymerization of the microtubules (Keeling et al. 2016).

Cilia are classified to three types: motile, immotile (primary), and nodal cilia. Motile cilia have 9+2 microtubule structure of nine outer microtubule doublets surrounding a central microtubule pair (Figure 1). Inner and outer dynein arms, radial spokes and central pair projections enable movement. They move actively: rapid forward movement is followed by slow recovery stroke (Ishikawa 2017). Cell types with motile cilia have usually several of them. In mammals, motile cilia are present on surface epithelial cells lining respiratory tract, brain ventricles and oviducts. Their primary function is to promote movement of fluids or substances, for example airway mucus, cerebrospinal fluid, and egg cells (Praveen et al. 2015). Animal sperm cell has a motile flagellum, which consists of 9+2 microtubule doublets and accessory structures. The flagella have similarities to axoneme of motile cilia. Same gene mutations often affect both motile cilia and sperm flagella, causing respiratory illnesses and male infertility (Sironen et al. 2011). Nonmotile primary cilia have 9+0 structure without the central microtubule pair and dynein

arms. They bend passively due to movement of fluid. Nodal cilia have 9+0 structure with dynein arms and have an ability for active movement. Nodal cilia are found in the embryo during gastrulation and are essential for developing left-right asymmetry of internal organs (Fliegauf et al. 2007).

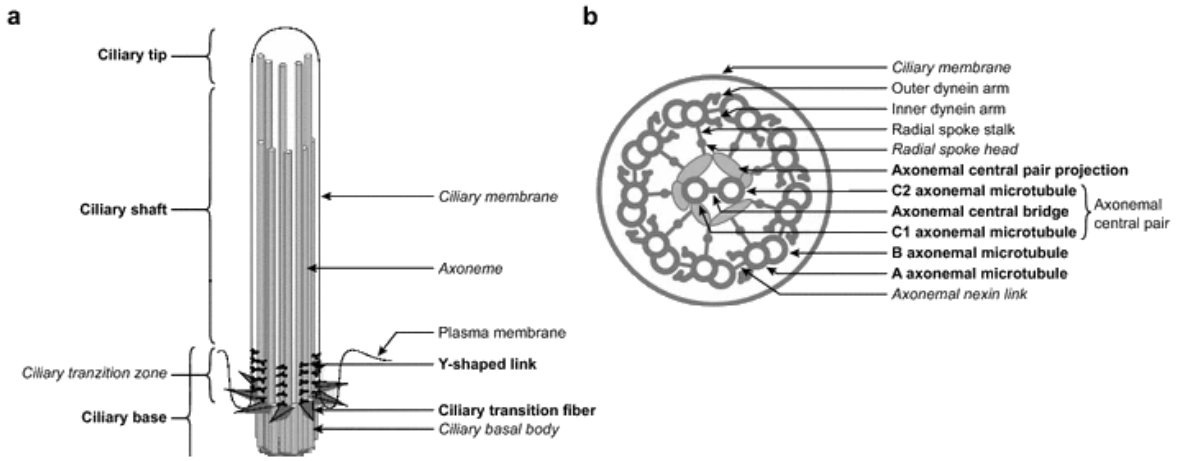

Figure 1. The structure of the eukaryotic motile cilium. Basal body anchors the cilium to the cell body. Primary and nodal cilia lack the central microtubule pair. (Adapted from Roncaglia et al. 2017). Copyright P. Roncaglia, T.J.P. van Dam, K.R. Christie et al. and BioMed Central Ltd. CC-BY.

Primary cilia are considered as a sensory organelle. They are found in cells that are in growth arrest. Sensory cilia are found in e.g. olfactory organs and vertebrate photoreceptors. Many organs and tissues have primary cilia, including kidney, liver, pancreas and brain. Primary cilia detect and transmit signals from environment to the cell body to regulate embryonic development and tissue homeostasis (Anvarian et al. 2019). A number of transmembrane receptors have been localized to the mammalian primary cilium, including the SSTR3 isoform of somatostatin receptor, the 5HT6 isoform of the serotonin receptor, Smoothened (SMO), a transmembrane receptor in the Hedgehog pathway, and the PDGFRα isoform of the platelet-derived groth factor receptor (Follit et al. 2006). Primary cilia are important for canonical Sonic hedgehog (SHH) signaling during embryonic development in vertebrates. Premature SHH signaling can disrupt skeletal morphogenesis. Ciliary G protein-coupled receptors (GPCR) regulate calcium levels and water reabsorption in renal epithelial cells. Most neurons in mammalian brain

have primary cilia. Defects in GPCR localization to the cilia are associated with neuropathologies (Anvarian et al. 2019).

Basal body anchors the cilium to the cell body. Basal body formation has two pathways. In the centriolar pathway, a pair of existing centriole serves as an organizing center for the duplication of new centrioles. In the acentriolar pathway, new centrioles are formed de novo from fibrous granules. Both pathways give rise to procentrioles, which mature as they migrate near the cell membrane, where they become basal bodies (Breslow and Holland 2019). The ciliary axoneme originates from the basal body, which is built of nine triplet microtubules. The basal bodies have additional structures, which assist them with anchoring into cell membrane. Transitional fibers emanate from the distal part of the basal body and contact the ciliary membrane. Together these membrane-contacting structures form ciliary pore complex that restricts vesicle and possibly protein entry to organelle (Silverman et al. 2009). Transition zone is localized at the base of the cilium, where it controls protein access to the cilium (Lechtreck 2015).

Intraflagellar transport (IFT) is a dynamic process that is responsible for the transport of proteins along the ciliary axoneme (Figure 2). Anterograde transport towards the ciliary tip is achieved by kinesin 2 motor, whereas retrograde transport towards the ciliary base is driven by dynein 2. IFT complexes facilitate the transport of protein complexes along the axoneme (Oh et al. 2012). Anterograde and retrograde IFT are required for cilia assembly. After cilia formation, IFT-based protein import and export are required for ciliary maintenance and signaling (Lechtreck 2015).

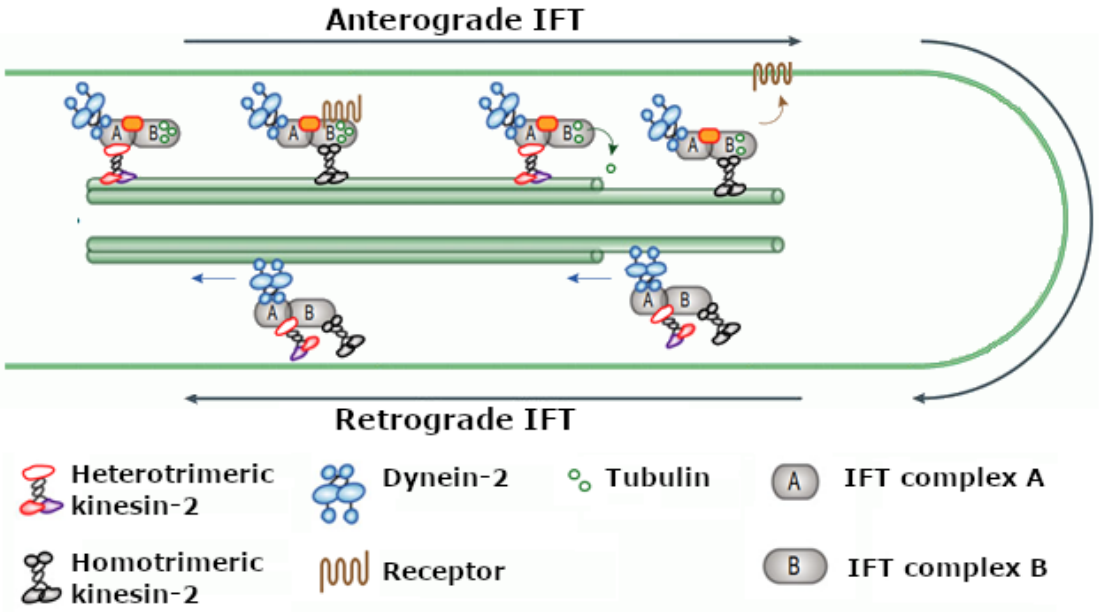

Figure 2. Intraflagellar transport. In anterograde IFT, motor protein kinesin 2 transports IFT complexes A and B, cargo proteins and inactive dynein-2 to the tip of the cilium. Cargo is released, and activated dynein 2 facilitates retrograde IFT. Membrane proteins are transported with IFT complexes. (Adapted from Prevo et al. 2017). Copyright B. Prevo, J.M. Scholey, E.J.G Peterman and the FEBS Journal. CC-BY.

Ciliogenesis is associated with the cell cycle (Figure 3). Primary cilium formation first occurs during G1 phase in which the centrosome migrates toward the cell

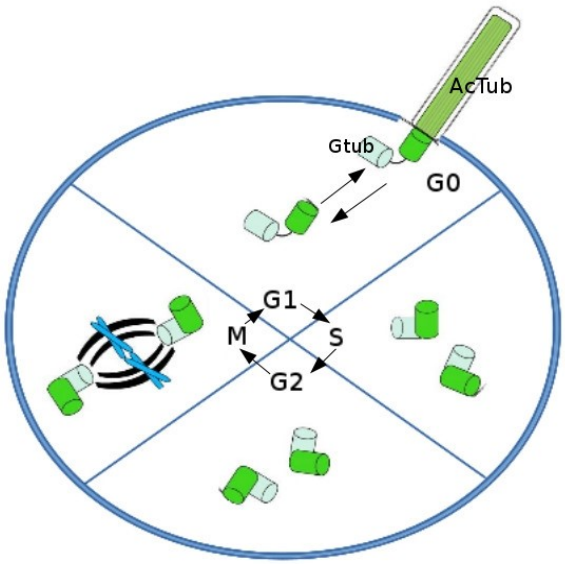

Figure 3. Cell cycle and ciliogenesis. At G1 phase, cell can exit cell cycle, differentiate and form a cilium (G0 phase). The cilium is resorbed, if the cell reenters the cell cycle. α-tubulin in the cilium is acetylated (AcTub). γ-tubulin (Gtub) localizes to centrosomes and ciliary basal body. (Adapted from Tsang and Dynlacht 2013). Copyright W.Y. Tsang, B.D. Dynlacht and BioMed Central Ltd. CC-BY.

membrane and initiates ciliogenesis (Malicki and Johnson 2017). Structural and transport proteins are activated to build the primary cilium axoneme. During the end of G1 phase, as well as in G0, the primary cilium functions as a receiver of sensing and interpreting signals from the extracellular environment. In S phase, the centrioles are duplicated. In late G2 phase centrioles reach maturity, and the primary cilium is disassembled prior to entrance to mitotic cell cycle and centrosome duplication for mitosis. In animals, immotile and motile cilia share similar structures, such as basal body and microtubule-based axoneme. Therefore cell lines with primary cilia can be utilized to study localization and function of genes expressed also in motile cilia and flagella (Girardet et al. 2019).

1.2 Ciliopathies

Ciliopathies are genetic disorders of the cilia or cilia anchoring structures, basal bodies, or of ciliary function. Since cilia are critical for organism development, homeostasis and reproduction, a wide variety of symptoms are potential clinical features of ciliopathies. Dysfunction of ciliated cells can lead to defective chemo- or mechanosensation. Cellular motility dysfunctions, displacement of cellular fluid and abnormalities in paracrine signal transduction are observed in many ciliopathies (Reiter and Leroux 2017).

Several inherited ciliary disorders result in renal cyst development. The most common form is autosomal dominant polycystic kidney disease (ADPKD). ADPKD affects between 1:1000 and 1:4000 individuals in EU, which makes it one of the most common genetic diseases in humans, and a significant cause of end-stage renal failure (Wheway et al. 2019) ADPKD is caused by mutations in *PKD1* or *PKD2* genes. The PKD1 protein, polycystin-1, is a receptor-like protein, whereas polycystin-2 is a transient receptor potential channel. Polycystins localize to primary cilia and may act as a mechanosensors in kidney tubule lining epithelia. Recessive polycystic kidney disease (ARPKD) is a neonathal form and is associated with enlarged kidneys and biliary dysgenesis. ARPKD is caused by mutation in

PKHD1, and truncating mutations are associated with perinatal lethality (Harris and Torres 2009). Other genes may cause similar symptoms for ADPKD and ARPKD. Kidney cysts are clinical features of some multi-organ ciliopathies, such as Meckel-Gruber syndrome and nephronophtitis (Table 1).

Table 1. Major ciliopathies and some examples of causative mechanisms. Many gene families are associated to multiple ciliopathies. Situs inversus is a criterion for Kartagener´s syndrome, but is not always manifested in PCD. (Reiter and Leroux 2017, Sorusch et al. 2019, Szymanska and Johnson 2012, Wheway et al. 2019.)

Ciliopathy	**Disease pathology**	**Mechanism(s)**
Alström syndrome	Retinitis pigmentosa, deafness, obesity, diabetes mellitus	Centriole, basal body
Bardet-Biedl syndrome	Retinal dystrophy, obesity, polydactyly, renal dysfunction, hypogonadism	Anterograde IFT, transition zone
Jeune syndrome, Asphyxiating thoracic dystrophy	Narrow chest, short ribs, arms and legs, polydactyly, renal abnormalities, hearth defects	Anterograde and retrograde IFT, transition zone
Joubert syndrome	Brain abnormalities, apnea, ataxia, distinctive facial features, developmental delay	Axoneme, cilium tip, transition zone, basal body
Meckel-Gruber syndrome	Encephalocele, polydactyly, polycystic kidneys, lethality	Axoneme, cilium tip, transition zone, basal body
Nephronophtitis	Cystic kidneys, liver fibrosis, retinal dysplasia	Axoneme, transition zone, basal body
Oral-facial digital syndrome type I	Malformations of the face, oral cavity and digits, kidney cysts	Axoneme, cilium tip, transition zone
Polycystic kidney disease	Polycystic kidneys	Ciliary membrane
Primary ciliary dyskinesia (Kartagener´s syndrome)	Respiratory infections, male infertility, otitis media, (situs inversus)	Motility apparatus, central pair, dynein arms
Retinitis pigmentosa	Retinal degeneration	Transition zone, anterograde IFT
Senior-Löken syndrome	Cystic kidneys, retinal degeneration	Centriole, basal body, transition zone
Usher syndrome	Retinal dystrophy, sensorineural hearing loss	Anterograde IFT

Malfunction of IFT is associated with many ciliopathies. IFT is essential for retinal visual cells. Outer segments of eye photoreceptor cells are specialized sensory cilia. Outer segment of a photoreceptor contains membraneous discs, which are continuously regenerated. Renewal depends on constant transport of rhodopsin and other visual pigments to outer segment (Bujakowska et al. 2017). Retinitis pigmentosa affects around 1:3500 people worldwide (Wheway et al. 2019). Mechanism of retinal degeneration varies. Cilium formation or length control is impaired, an enzyme that lowers ciliary cGMP concentration is defective, or rhodopsin or other phototransduction components are mislocalized (Reiter and Leroux 2017). *RPGR* is a ciliary transition zone gene. Transition zone regulates the access of IFT complexes to the cilium. Mutations in *RPGR*, which localizes to photoreceptor connecting cilium, account for 20% of retinitis pigmentosa cases. Retinal degeneration is observed in 20% of nephronophtitis cases, and it is a main feature of Bardet-Biedl syndrome (Fliegauf et al. 2007). BBSome, MKS, and NPHP are protein complexes located to transition zone. Mutations in genes coding transition zone proteins cause Bardet-Biedl, Meckel-Gruber and Joubert syndromes, and nephronophtitis (Parisi 2019).

Basic ciliary functions are relatively conserved between tissues. Therefore many sensory ciliopathies affect multiple organs. Reduced sense of smell (hypoosmia, anosmia) is frequently observed in Bardet-Biedl patients. In olfactory cells, mistrafficing of ciliary protein impairs their function (Reiter and Leroux 2017). Loss of hearing and balance are symptoms of Usher syndrome, which affects kinocilia in inner ear (Mathur and Yang 2015). Primary cilia and IFT are required for mesenchymal stem cells to differentiate to chondrocytes and osteoblasts. Some primary ciliopathies cause skeletal dysplasias, such as Jeune syndrome and short-rib polydactyly type III (Yuan et al. 2015).

Defect in motile cilia function, primary ciliary dyskinesia (PCD) affects approximately 1:15 000 people. PCD is genetically heterogenous. In sperm flagella, dyskinesia and morphological abnormalities may result in male infertility (Cindric

et al. 2020). Not all PCD mutations cause male infertility, thus there are differences in protein content and function between motile cilia and sperm (Sironen et al. 2019). Motile cilia are present in middle ear and respiratory epithelial cells from sinuses to conducting bronchioles. Ciliary dyskinesia prevents mucus clearence in airways, and therefore causes chronic sinusitis, recurrent otitis media, and bronchiestasis (Stillwell et al. 2011). Occasionally ciliary motility in oviduct is decreased, and improper oocyte transport may lead to female subfertility. Oviduct cilia are similar to respiratory tract cilia, but not crucial for oocyte transport. A rare PCD symptom is hydrocephalus, which presumably results from impaired cereprospinal fluid movement by ependymal cilia (Reiter and Leroux 2017). Approximately 50% of PCD patients have dextrocardia and situs inversus totalis, in which major visceral organs are mirrored from their normal positions. Situs inversus is a criterion for Kartagener´s syndrome. Normal arrangement of internal organs is known as situs solitus (Stillwell et al. 2011). Abnormal positions of internal organs are caused by dyskinesia in embryonic nodal cilia. Nodal cilia are motile, but lack central microtubule pair in axoneme. Mutations in central pair-associated proteins can cause PCD without affecting situs (Cindric et al. 2020).

PCD has been associated with several genes encoding ciliary structures. Structural abnormalities have been documented with electron microscopy in inner and outer dynein arms, central pair and radial spokes. PCD genes also include cytoplasmic proteins required for dynein arm assembly (Reiter and Leroux 2017). Mouse models have been developed to carry mutations in these loci. They demonstrate aspects of the disorder, particularly rhinitis, sinusitis and abnormal situs. Most PCD models show additional symptoms to those commonly seen in PCD patients. Hydrocephalus is common in knockout mice, and cardiac defects have been reported (Norris et al. 2012). Tissue-specific knockout gives an opportunity to study animal models in fertile age, since embryonic development is not disrupted and individuals are likely to survive. Perinatal lethality of animal models can be avoided

with conditional deletions, which are chemically induced in adult animals (Ostrowski et al. 2010).

1.3 Cell models for ciliopathies

Mouse kidney epithelial cells (mIMCD3) are a traditional cell line for modeling ciliopathies, as they ciliate *in vitro* and are relatively easy to transfect. Other common cell lines include mouse fibroblasts (NIH/3T3) and human retina-pigmented epithelium cells (hTERT-RPE1). These cell types have a single primary cilium. There are no adherent immortaliced cell lines with motile cilia. Unicellular flagellated organisms, for example Chlamydomonas reinhardtii, serve as models for cilia motility. Ciliary dyskinesia can be studied on *ex vivo* cultures, such as mouse tracheal explants, or nasal brush samples from patients with PCD (Wheway et al. 2019, 100 000 genes project). Normal Human Bronchial Epithelial (NHBE) 3D cell cultures can be utilized for *in vitro* studies of cilia motility. Ciliary beat frequency is recorded by imaging apical surface (Rayner et al. 2019).

Generation of IMCD cell lines stably expressing fluorescent protein fusions on cilium proteins has been an important element of mammalian IFT protein imaging (Tran et al. 2008). The first IFT protein localized in Golgi complex was SPEF2 interacting protein IFT20, expressed in mIMCD3 line. Earlier IFT proteins characterized had been found localized to cilia and to the peri-basal body region within the cell body. GFP-tagged IFT20 is actively transported in the cell body and along the cilium in mammalian cells (Follit et al. 2006).

Major steps of cell line generation are building a construct containing fluorescent fusion protein cDNA, transfection of target cells, and clonal selection and characterization. Level of expression should be moderate: at high concentrations fluorescent-tagged proteins can form aggregates interfering with IFT imaging and cell viability. It is essential to ensure the fidelity of localization of the fusion protein

and absence of unintended artifacts with colocalization studies (Besschetnova et al. 2009).

For the visualization of primary cilium IFT particle movement and velocity, cells are imaged in their quiescent state when they reach the highest frequency of ciliation. This state can be achieved by contact inhibition of cell division, when cultured to 100% confluency or by serum starvation. Live cells are imaged with inverted microscope as a time-lapse series. The cilium tip has usually the brightest intensity, which helps to identify the direction of particle movement, anterograde versus retrograde (Besschetnova et al. 2009).

1.4 Sperm development

Spermatogenesis in mammals occurs in seminiferous tubules of the testis. Spermatogenesis is divided in three phases: mitosis, meiosis and spermiogenesis. In phase 1, spermatogonia undergo several mitotic divisions to form spermatocytes. In phase 2, spermatocytes undergo two meiotic divisions to form haploid spermatids. In phase 3, spermatids develop into spermatozoa through a complicated metamorphosis (Hess et al. 2008). Spermiogenesis involves structural modifications including nucleus reshaping, chromatin condensation, organelle reorganization, acrosome formation, and flagellum formation (Hermo et al. 2010 part 1).

Spermatogenesis is a cyclic process. Mouse spermatogenesis consists of 12 stages (Figure 4), according to cellular associations observed in tubular cross sections and visualized by the periodic acid-Schiff´s reaction (PAS). Germ cells within each layer of the seminiferous epithelium change in synchrony with the other layers over time. An order of the stages is observed, stages occur with repetition along the length of the tubules, in a wave of the seminiferous epithelium. In mice, duration is 8.6-8.9 days for each cycle and 39-40 days for spermatogenesis to complete (Hess et al. 2008). In addition to germ cells, Sertoli cells are present in the seminiferous tubules.

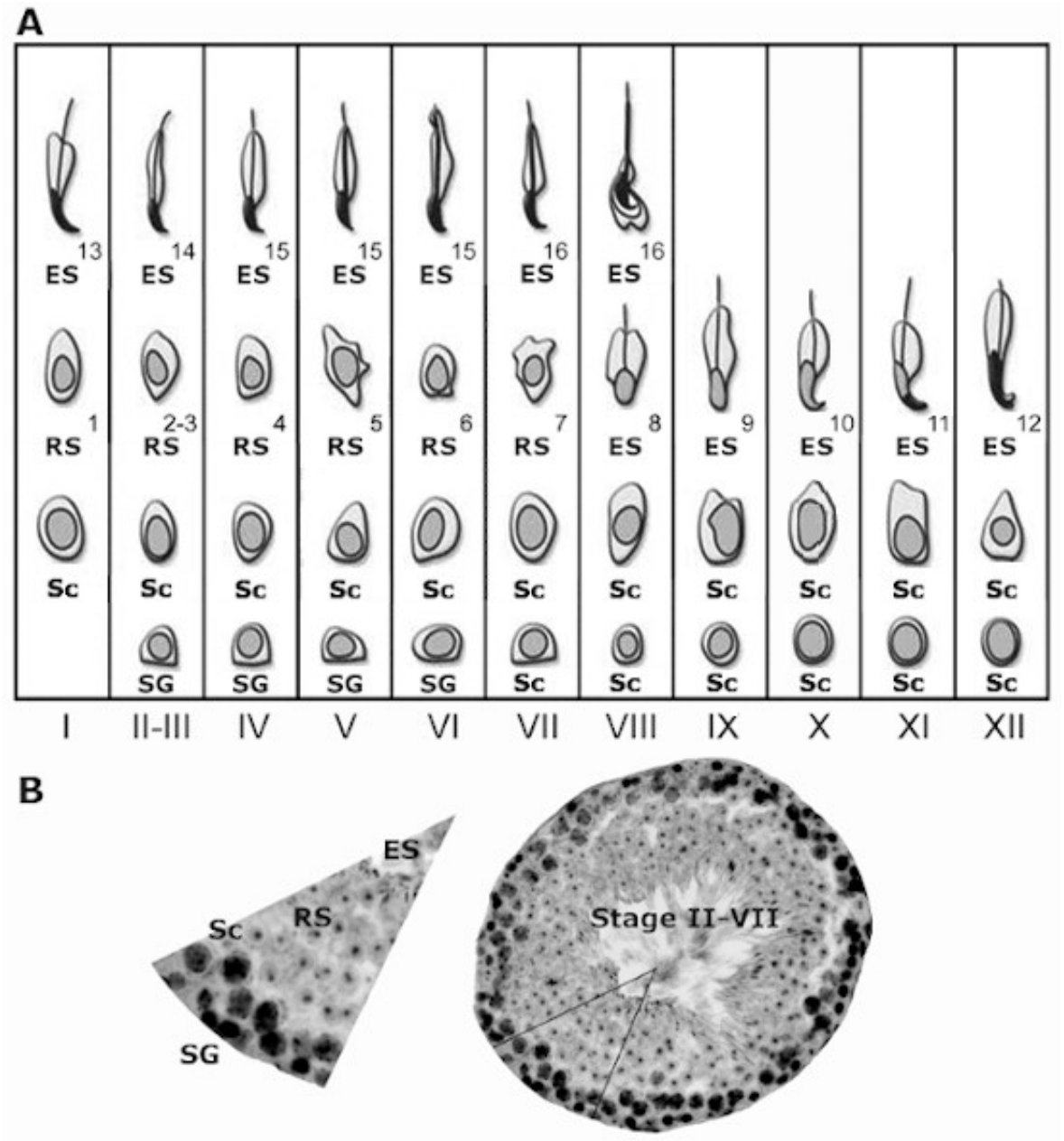

Figure 4. Mouse spermatogenesis. (A) Schematic representation of the seminiferous epithelial cycle of the mouse. Roman numbers represent the stage of the seminiferous epithelium. Spermiogenesis is divided to 16 steps. SG, spermatogonia; Sc, spermatocytes; RS, round spermatids; ES, elongating spermatids (Adapted from Kent and Griswold 2014.) Copyright T. Kent, M.D.Griswold and the MDPI Journals. (B) Cross section of seminiferous tubule in the mouse testis. Different germ cell types are observed in magnification of the tubule. The nuclei are visualized with DAPI, cell bodies with acetylated α-tubulin. Black-and-white adaptation. Copyright U.M. Sahinaho.

Sertoli cells secrete hormones and growth factors to nourish developing sperm cells. They also act as phagocytes. Sertoli cells are connected to each other by tight junctions, which form a protective blood-testis barrier (Franca et al. 2016).

Elongating spermatids contain a transient a microtubular platform, the manchette, which transports proteins during spermiogenesis. Intramanchette transport (IMT) resembles IFT, and many IFT proteins localize to the manchette (Lehti et al. 2017). Structural proteins are transported through IMT to the basal body of the spermatid, and further delivered to the developing sperm tail by IFT (Lehti and Sironen 2016). In mice, the manchette begins to form in step 8 spermatids, when the shape of the nucleus starts to elongate. Later, at steps 11-13 the manchette undergo a transition from a symmetric cylindrical microtubule array to an asymmetric configuration (Hermo et al. 2010 part 2). Defects in manchette formation and function lead to defects in the morphology of the nuclei: instead of their normal slender shape they have irregular, often knobbed-like appearance (Lehti and Sironen 2016).

Sperm flagellum is structurally divided to the connecting piece, the midpiece, the principal piece, and the end piece (Figure 5). The axoneme of the flagellum has 9+2 microtubule structure, similar to motile cilia. Inner and outer dynein arms provide motor force needed for flagellar beating. The midpiece and principal piece have

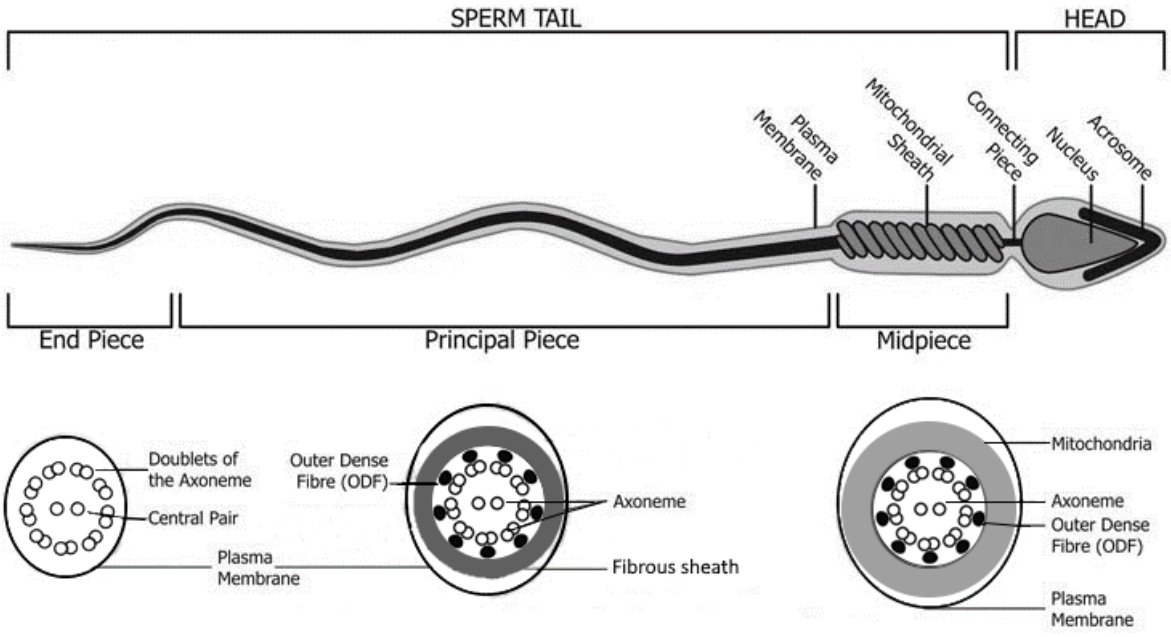

Figure 5. Schematic view to mammalian sperm. The axoneme of sperm tail has 9+2 microtubule structure, similar to motile cilia. Outer dense fibers run along the middle and principal piece of the sperm tail. Fibrous sheath supports the principal piece. Mitochondria are located to the middle piece. (Adapted from Borg et al. 2010). Copyright C-L. Borg, K.M. Wolski, G.M.Gibbs, M.K. O`Bryan and the Oxford Journals. CC-BY.

outer dense fibers, which stabilize the axoneme to maintain sperm motility. Mitochondria are located to the midpiece. Fibrous sheath in the principal piece contains glycolytic enzymes. Mouse spermatozoa utilize glycolysis as well as oxidative phosphorylation to produce ATP as an energy source (Buffone 2012).

1.5 Sperm flagellar protein 2

Immotile short-tail sperm (ISTS) defect in pigs was detected in Finnish Yorkshire boars in 1987. The ISTS phenotype is characterized as lower sperm counts, short sperm tails, and disrupted axonemal structures (Andersson et al. 2000). ISTS is caused by insertion of LINE1 transposon within the intron 30 of *Spef2* gene (Sironen et al. 2006, 2007). Insertion creates altervative splicing site, which introduces the stop codon in mRNA and leads to degradation of the mRNA through nonsense mediated decay. SPEF2 expression is tissue-specific. ISTS affects only testis-specific isoform and causes male infertility (Sironen et al. 2006). SPEF2 is highly conserved in mammals: amino acid sequence identity is 69 % for mouse and human, and 68 % for mouse and pig (UniProt database, BLAST search). Recently, *Spef2* mutations have been identified to cause male infertility with PCD-like symptoms (Tu et al. 2020).

Mouse *Spef2* gene comprises of 43 exons (Sironen et al. 2010). Several conserved domains have been predicted for SPEF2 including a calponin homology domain from amino acids 5 to 136 and adenylate kinase (ADK) domain from amino acids 618-800 (NCBI Conserved domain search, Sironen et al. 2011). Adenylate kinase are enzymes, which function in many ciliary and flagellar systems to regenerate ATP from ADP in a nucleotide phosphoryl exchange reaction 2ADP ↔ ATP + AMP. A distinct role for adenylate kinase is emerging in cell motility, differentiation and mechanoelectrical signal transduction. Adenylate kinase has been implicated in spermatozoa motility by facilitating ATP delivery from midpiece mitochondria to remote ATPases in the tail (Dzeja and Terzic 2009). A calcium-binding EF-hand motif has been predicted from porcine homolog (Sironen et al. 2006). Domain of

unknown function DUF1042 classifies SPEF2 together with other proteins implicated in flagella function, such as mouse SPEF1, and CPC1 of Chlamydomonas reinhardtii. One conserved domain within CPC1 is homologous to adenylate kinases. Mutations at *CPC1* gene disrupt assembly of a part of the central pair complex. Knocking out *CPC1* in cell culture reduces ciliary beat frequency (Zhang and Mitchell 2004).

C-terminal part of SPEF2 interacts with intraflagellar transport protein IFT20, which localizes to Golgi complex and cilia in ciliated cell lines (Figure 6) (Sironen et al. 2010). One of the possible roles of SPEF2 is in intramanchette transport in elongating spermatids, and intraflagellar transport in other tissues (Lehti and Sironen 2016). Some interacting partners have been identified in male germ cells. SPEF2 functions in microtubule-mediated transport with dynein-1. Cytoplasmic dynein 1 complex mobilizes SPEF2 in elongating spermatids. Dynein seems to be required for SPEF2 transport in the manchette. Golgin subfamily A member 3 (GOLGA3) and SPEF2 colocalize in Golgi complex indicating a possible interaction sites. GOLGA3 localizes to Golgi in spermatocytes and round spermatids (Lehti et al. 2017). In

A

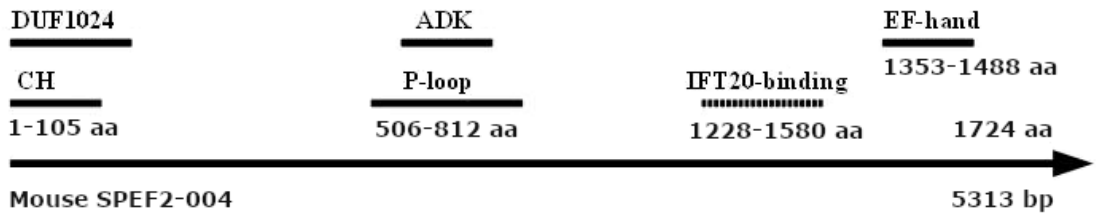

B

Transcript name	Base pairs	Protein aa	Mw kDa
SPEF2-001	4247	875	100
SPEF2-002	1917	622	73
SPEF2-003	1422	456	54
SPEF2-004	5313	1724	198
SPEF2-005	1639	513	61
SPEF2-006	7038	2076	237

Figure 6. (A) Mouse SPEF2 canonic sequence, SPEF2-004. Predicted domains are shown. CH, Calponin Homology; DUF, Domain of Unknown Function; ADK, Adenylate Kinase; P-loop, Phosphate-binding loop; IFT20-binding domain; EF-hand, calsium-binding motif. (Sources: Ensembl database, Uniprot database) (B) Mouse SPEF2 transcripts and predicted molecular weights. (Adapted from transcript table by Ensembl database 2020.)

human respiratory epithelial cells, SPEF2 is associated with central pair protein HYDIN (Cindric et al. 2020).

SPEF2 is expressed in many ciliated tissues. Long isoform of SPEF2 is expressed in the testis. Shorter forms have been detected in the lung, brain, kidney and liver, but not in the heart (Sironen et al. 2010). SPEF2 is expressed in bone and cartilage, and its depletion impairs osteoblast differentiation, resulting in bone formation defects (Lehti et al. 2018). During spermatogenesis, the SPEF2 protein has been shown to localize in step 10-12 elongating spermatids in the manchette, in the basal body at steps 13-14 and in the midpiece of sperm flagella at steps 14-16. SPEF2 is also present in Sertoli cell cytoplasm (Sironen et al. 2010).

Loss of SPEF2 function leads to primary ciliary dyskinesia in mice. Mice homozygous for the mutation *big giant head (bgh*) have several abnormalities associated with PCD, including hydrocephalus, male infertility and sinusitis. *bgh* mice have *Spef2* mutations in exon 3 and exon 28. Male infertility in *bgh* mice is caused by shortened flagella and disorganized axonemal and accessory structures in elongating spermatids and mature sperm. Respiratory cilia are ultrastructurally normal, but their beat frequency is lower than in wild-type cilia. Hydrocephalus can cause postnatal lethality. Sperm defects in *bgh* mice resemble porcine ISTS phenotype. In Yorkshire boars and *bgh* mice, mutations prevent expression of long SPEF2 isoform in male germ cells (Sironen et al. 2011).

1.6 Aims of the study

First aim of the study was to produce a novel antibody against SPEF2 protein and analyze SPEF2 expression and localization with ciliated cells. Tissue samples were obtained from wild-type and *Spef2* knockout mice. Antibody was tested in Western blot and immunofluorescence experiments.

Second aim was to elucidate SPEF2 function in ciliated cells. Mouse epithelial kidney (mIMCD3) cells were transfected with SPEF2 fragments attached to green

fluorescent protein (GFP). Fragments represented different domains of SPEF2. This study compared, which domains are essential for SPEF2 localization and transport to cilia.

2 MATERIALS AND METHODS

2.1 Fusion protein for antibody production

KAD fragment of SPEF2 included aminoacids 550-850 from testis-specific SPEF2 protein (Appendix 1). KAD fragment was cloned mouse testis cDNA and joined to pGEMX-4T2 vector between BamHII and SaII sites. Construct was transformed to BL-21 Codon Plus (DE3)-RIPL electrocompetent E. coli cells. Transformed cells were provided by Dr. Mari Lehti, LUKE.

Cells were thawed from glycerol stock and grown in 1.5 ml LB + ampicillin in 37°C 160 rpm. Volume was increased to 25 ml and grown n 37°C 160 rpm o/n. Volume was increased to 250 ml and grown n 37°C 160 rpm 3h. Production was induced with 0.1 mM IPTG and grown 37°C 160 rpm 4h. Bacteria were centrifuged 6000 rpm 15 min +4°C with Sorvall SLA-1500 rotor. Pellet was suspended with BugBusterTM Protein Extraction Reagent (NOVAGEN), 2,5 g bacteria/5 ml BugBuster, 1 µl/ml Benzonase + rLyzozyme. Suspension was incubated end-over-end 20 min RT. Lysate was centrifuged 16 000g 20 min +4°C. Affinity chromatography was performed with BugBuster GST column. Column was balanced with GST bind & wash buffer. Lysate was run through the column. Column was washed twice with GST bind & wash buffer. Column was eluted with 15 mM elution buffer and 3 x 1,5 ml fractions were collected. Fractions were analyzed in SDS-PAGE. 25 µl of sample was combined with equal volume of sample buffer. Buffer (0,125M Tris, 4% SDS, 20% glycerol, 10% 2-mercaptoethanol, 0.004% bromophenol blue) was added to the lysate/eluate and denaturated +85°C 3 min. Proteins were separated in 8%

acrylamide gels with BioRad TetraCell electrophoresis apparatus. Run settings were 100V, 80 mA, 8W. Protein was sent for further purification and anti-Mouse antibody production in rabbit. Antibody was manufactured by Abnova, Cat#1204000270.

2.2 Western blot

Mouse tissues were provided by Dr. Mari Lehti, LUKE. Frozen tissues were transferred to lysis buffer (50 mM Tris-HCl pH 8.0, 170 mM NaCl, 1% Triton-X 100, 5 mM EDTA, 1 mM DTT, 1X protease inhibitor coctail (Roche) in mQ-H2O) and lyzed using Tissuelyzer (Qiagen) 30 sec 50 Hz. Lysates were incubated on ice 20 min, then centrifuged 13 000 x g 40 min at +4°C. Protein concentration was measured with Pierce BCA method. BSA standards and sample buffers were prepared according manufacturer´s protocol (Thermo Fisher Scientific). 6,25 µl of each standard/sample was transferred to PCR tubes. 50 µl of working reagent was added to tubes, then mixed gently and spinned. Tubes were incubated 30 min at +37°C, then cooled at RT. Tubes were mixed and spinned. Concentration was measured at Nanodrop, sample volume 2 µl.

Loading buffer (0,125M Tris, 4% SDS, 20% glycerol, 10% 2-mercaptoethanol, 0.004% bromophenol blue) was added to the tissue lysate and denaturated +95°C 5 min. Proteins were separated in 8% acrylamide gels with BioRad TetraCell electrophoresis apparatus. Run settings were 100V, 80 mA, 8W. Voltage was raised for lower gel to 120V. Proteins were transferred to nitrocelluloce membrane with BioRad Semidry system. Run settings 15 V, 200 mA, 5 W. Unspecific sites were blocked in 5% non-fat milk in PBS containing Triton X-100 at 0.1% (PBST) 2h or o/n. Membrane was washed briefly in PBST. Primary antibodies were diluted in 1% non-fat milk/ PBST. Anti-FLJ (Abnova), and anti-SPEF2-KAD (Abnova) were diluted 1:500, anti-acetylated/non-acetylated α-tubulin (Sigma-Aldrich) 1:2000. Incubation was carried in rotation +4°C o/n. Membrane was washed 4x10 min in PBST. Secondary antibodies were diluted 1:4000 1% non-fat milk/ PBST. HRP-conjugate (BioRad) was added diluted to secondary antibody 1:15 000. Amersham ECL Prime

Western Blotting Detection Reagent (GE Healthcare) was used for detection. Membranes were photographed with FluorchemQ Imaging System without filter, sensitivity set to medium, and exposure times from 8 to 12 min.

2.3 *Spef*2 mouse model

*Spef*2 knockout mouse samples were received from LUKE. *Bgh* mouse mutant was generated by N-ethyl-N-nitrosourea mutagenesis on the C57BL/6J background mice and maintained on a mixed C57BL/6J;C57BL/10J background (Sironen et al. 2011). *Spef*2 full KO mice lack exons 3-5 and have a stop codon after exon 2 (Table 2, Lehti et al. 2018).

Table 2. Spef2 knockout mouse strains.

Knockout	**Genotype**	**Phenotype**	**Reference**
*Spef*2 KO	Deletion of exons 3-5, stop codon after exon 2	Hydrocephalus, growth retardation, bone formation defects, death prior to 5 weeks age.	This study, Lehti et al. 2018
big giant head	Missense mutation in exon 3, nonsense mutation in exon 28	Male infertility, sinusitis, hydrocephalus. Death on average at 3,5 weeks age.Genetic background affects severity of hydrocephalus.	Sironen et al. 2011, Finn et al. 2014
*Spef*2 cKO	Conditional deletion of exons 3-5 in male germ cells	Male infertility, multiple sperm structural defects, such as short flagella, basal body duplication, abnormal sperm head shape.	Lehti et al. 2017
*Spef*2 KO	Deletion of exons 3-6	Male infertility, female subfertility/infertility, sinusitis, hydrocephalus. Majority die around 5 weeks age, ~20% reach fertile age.	Tu et al. 2020

Bacterial artificial chromosome (BAC) construct was used to transfect hybrid mouse embryonic cells. Blastocysts were implanted into pseudopregnant female surrogate mouse at 15 weeks age. Chimeric mice were bred with wild-type mice to produce heterozygous animals. Two heterozygotes were bred to achieve homozygous *Spef*2 full KOs. Homozygotes have been phenotyped, and heterozygous mice have been

used to develop tissue-specific knockouts. Majority of full KO mice die at 5 weeks age. Few individuals lived to fertile age and adult testis samples were received (Lehti et al. 2018).

2.4 Tissue sections

Paraffin sections of wild type and knockout mice tissues were prepared at University of Turku. Sections were deparaffinized in xylene 2x5 min, 100% ethanol 2x3 min, 95% ethanol 1 min, 70% ethanol 1 min, then rinsed with distilled water. Sodium citrate buffer (10nM Sodium Citrate, 0.05% Tween 20, pH6) was pre-heated to +95°C. Slides were incubated 20 min in citrate buffer. Slides were allowed to cool at RT 20 min, then rinsed with PBS 2x2 min. Sections were blocked with 5% NGS. Primary antibodies, anti-acetylated α-tubulin (Sigma-Aldrich) 1:2000, anti-SPEF2-KAD (Abnova, Cat# 1204000270) 1:500 were diluted in PBST + 3% NGS and incubated at +4C overnight. Sections were rinsed in PBS-Tween 20 2 x 2 min. Secondary antibodies anti-Mouse Alexa Fluor 488 and anti-Rabbit 555 (Invitrogen) were diluted in PBST + 3% NGS 1:500. Sections were incubated with secondary antibody 1h RT. Slides were rinsed in PBS-Tween 20 3 x 2 min, mounted with DAPI and covered with glass. Sections were photographed with EVOS fl inverted fluorescence microscope.

2.5 Immunofluorescence of male germ cells and sperm slides

Stage-specific segments of adult C57BL/6NHsd mouse seminiferous tubules were prepared with drying-down method. Segments were isolated and transferred in 20 µl of 100 mM sucrose solution in a small Petri dish. Cells were released from tubules by squeezing carefully with fine forceps and were then suspended by gentle up-and-down pipetting. The cell suspension was spread on a slide dipped in the fixing solution (1% paraformaldehyde [PFA]) 0.15% Triton X-100 [pH 9.2]), and slides were dried overnight in a highly humidified box.

Epididymal sperm samples were spread on glass slides and let air-dry. Drying-down samples and sperm samples were fixed with 4% PFA 15 min, then washed 2 x 5 min in PBS. Slides were incubated in 0,2% Triton-X 100 in PBS 10 min, then washed 2 x 5 min in PBS. Slides were blocked in 10% NGS 1h RT. Primary antibodies, anti-acetylated α-tubulin (Sigma-Aldrich) 1:2000, anti-SPEF2-KAD (Abnova) were diluted in PBS-Tween 20 + 3% NGS and incubated at +4°C overnight. Sections were rinsed in PBS-Tween 20 3 x 5 min. Secondary antibodies anti-Mouse Alexa Fluor 488 and anti-Rabbit 555 (Invitrogen) were diluted 1:500 in PBST + 3% NGS. Sections were incubated with secondary antibody 1h RT. Slides were rinsed in PBS-Tween 20 3 x 5 min, mounted with DAPI and covered with glass. Sections were photographed with EVOS fl inverted fluorescence microscope.

2.6 Transfection of mIMCD3 cells

mIMCD3 cells were grown in D-MEM/F12 medium (Invitrogen) with 10% FBS. Cell culture was maintained in +37C 5% CO2 incubator. Cells were transfected with three SPEF2-GFP constructs in pcDNA3.1/CT-GFP-TOPO plasmid containing sequences 5´testis, 3´-testis and KAD (Appendix 2). Sequences of the constructs were based on testis-specific SPEF2 isoform. Constructs were provided by Mervi Mutikainen, LUKE. Cell lines with different transfections were handled separately.

Cells were subcultured to 24-well plate in 500 µl of medium. 75 000 cells were transferred per well and grown o/n. 500 ng of plasmid was diluted in 100 µl D-MEM/F12 without serum. Transfection was done by lipofection with Lipofectamine kit (Invitrogen) containing LFX and PLUS Reagents. 0.5 µl of PLUS Reagent was added to the diluted DNA, mixed gently and incubated 5 min RT. 1,5 µl of Lipofectamine Reagent was added to diluted DNA, mixed gently and incubated 30 min RT. Expression Control Plasmid pcDNA3.1/CTGFP (Invitrogen, c=0,5 µg/µl) was used as transfection control. Cells were grown at +37°C for 24h to 90% confluency. Cells were either diluted 1:10 in growth medium with serum and transferred to bigger volume for an antibiotic selection, for which 200 µg/ml of

Geneticin G-418 sulphate (activity 706 µg/mg, Gibco Life Technologies) was added to growth medium, or detached with cell scraper and sent to fluorescence-activated cell sorting.

2.7 Fluorescent staining of mIMCD3 cells

Transfected cells were grown in 12- or 24-well plates to 90% confluency, then serum-starved in serum-free D-MEM/F12 24h. Cells were rinsed 3 x with PBS. Cells were fixed 20 min +4°C and rinsed 3 x PBS. They were permeabilized with buffer (2% NGS, 10 mg/ml BSA, 0.3% Triton X-100 in PBS) 30 min RT. Rinsed 3 x with PBS. Blocking was in buffer (5% NGS, 10 mg/ml BSA in PBS) 1 h RT. Cells were rinsed 3 x with PBS. Primary antibodies anti-acetylated α-tubulin 1:2000 (Sigma-Aldrich), anti-SPEF2-KAD 1:500 (Abnova), anti-γ-tubulin 1:1000 (Abcam) were diluted in binding buffer (2% NGS, 10 mg/ml BSA in PBS) and incubated 2h RT or O/N in +4°C. Anti-GFP antibody 1:500 (Invitrogen) was used to detect GFP constructs and amplify signal.

Medium was aspirated and cells washed 3 x with PBS 5 min on shaker. Secondary antibodies anti-Mouse Alexa Fluor 488 and anti-Rabbit 555 (Invitrogen) were diluted 1:500 in binding buffer. Cells were incubated with secondary antibody 1h at RT, then washed for 10 min in PBS on a shaker. Cells were mounted with mounting medium containing DAPI (Sigma-Aldrich) for nuclear staining and covered with a glass plate. Cells were photographed with EVOS fl inverted fluorescence microscope. Secondary antibody for anti-GFP was Alexa Fluor anti-rabbit 555 (1:500), which was imaged in red channel.

3 RESULTS

3.1 Fusion protein for antibody production

KAD fragment of SPEF2 was produced in E. coli and purified by affinity chromatography. A specific 66 kDa band was detected on SDS-PAGE of eluate (Figure 7). KAD fragment contains aminoacids 550-850 from testis-specific SPEF2 protein. Predicted molecular weight is ~66 kDA, which product corresponded to. Purified fragment served as an antigen in SPEF2 antibody production.

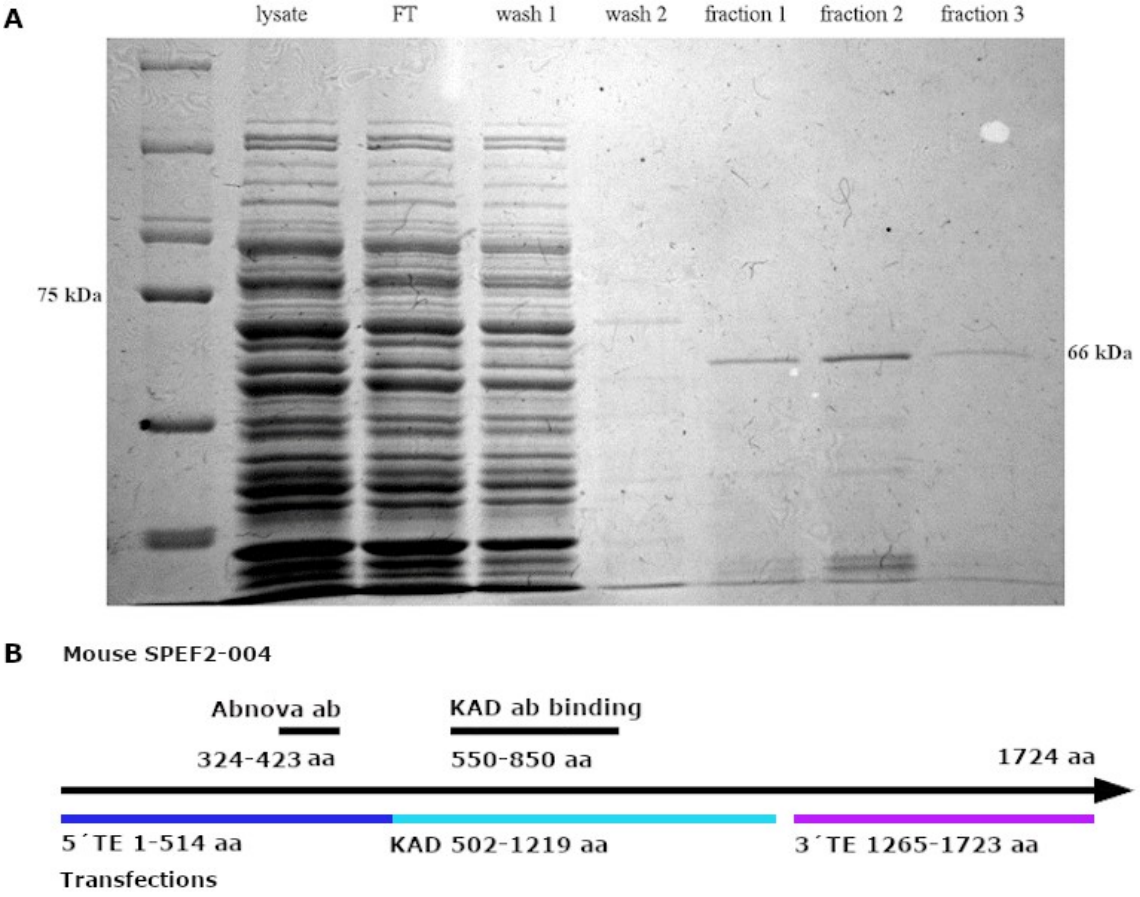

Figure 7. (A) KAD fragment purification for antibody production. (B) Schematic representation of designed antibody binding sites within SPEF2 protein. KAD antibody was utilized in Western blot and immunofluorescence in this study. Abnova antibody was used in Western blot. 5´TE, KAD and 3´TE fragments represent sequences transfected to mIMCD3 cells.

3.2 Western blot

SPEF2 expression in wild-type mouse testis lysates at different ages was investigated with novel KAD antibody. When spermatogenesis is initiated, different germ cell populations are observed in adolescent mice, and therefore SPEF2 expression changes during first weeks. Predicted molecular weight of SPEF2 is 200 kDa. KAD antibody detected ~250 kDa band in the testis at age of two weeks. Second band, molecular weight ~200 kDa, was present in testis, but absent in epididymis (Figure 8A). The difference between predicted and observed molecular weight could be caused by post-translational modifications.

Tissue lysates of WT mouse tissues were stained against SPEF2 with KAD antibody. A band with molecular weight ~250 kDa was detected in lung and oviduct, but not in kidney, or brain. In the brain was a strong ~120 kDa band, which was not observed in other tissues (Figure 8B). Several other bands were detected, which could be unspecific binding or shorter SPEF2 isoforms.

Expression of SPEF2 in WT testis was compared to *bgh* mutant and two *Spef2* KO mice. ~250 kDa and 200 ~kDa bands were observed in wild-type testis, but absent in *bgh* and KOs (Figure 8B). WT and KO tissue lysates were also tested with another anti-SPEF2 antibody (Abnova) binding to N-terminus. Faint ~250 kDa and 200 ~kDa bands were present in wild-type testis. These bands were absent in in *bgh* and KO tissues (Figure 8C).

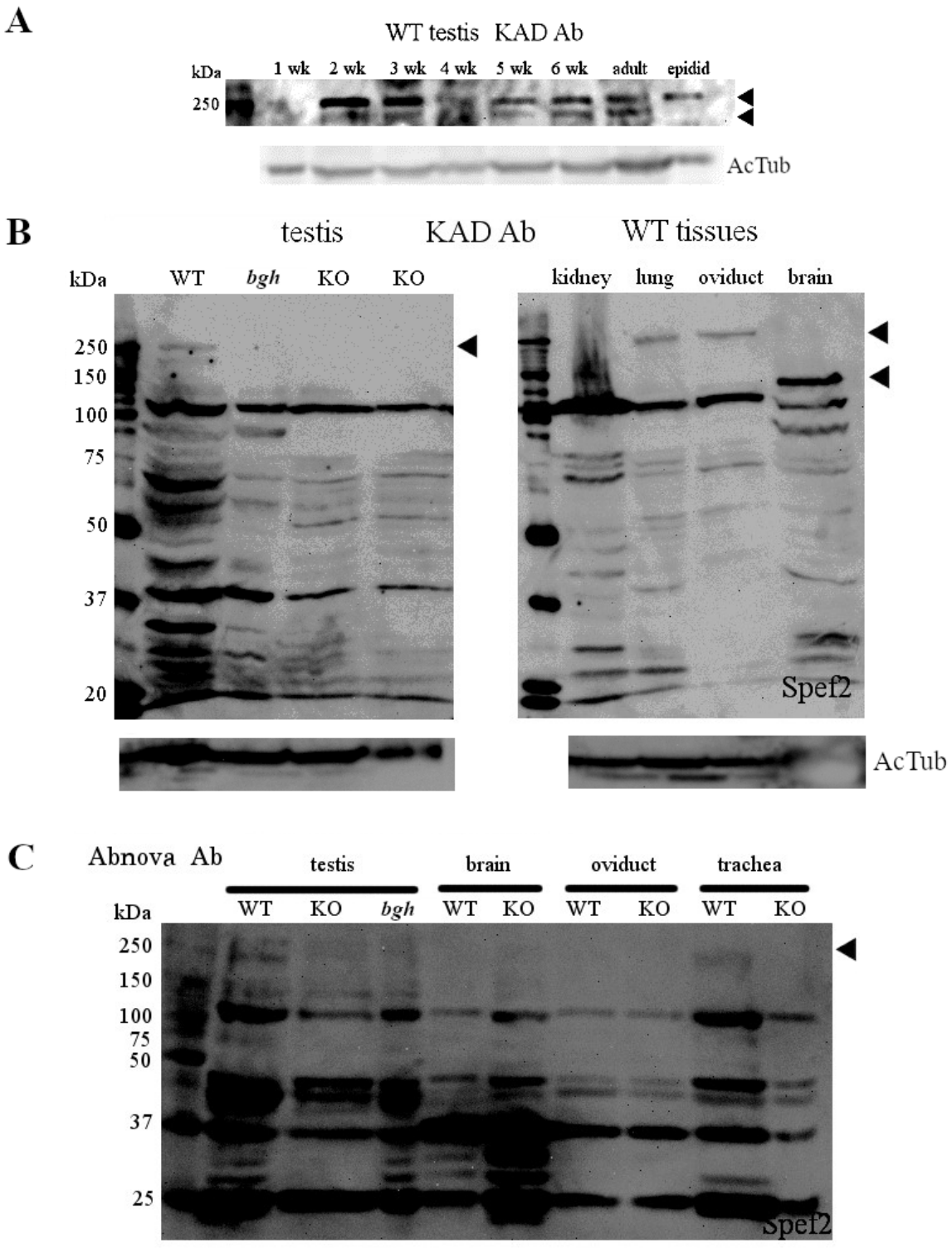

Figure 8. Western blot of mouse tissue lysates with KAD and Abnova antibodies. (A) KAD antibody. SPEF2 expression was observed in wild-type testis at different ages, and in adult epididymis. (B) KAD antibody. SPEF2 expression in the wild-type testis was compared with *bgh* mutant and two knockout samples. KAD antibody was also tested in ciliated wild-type tissues. (C) Abnova antibody. SPEF2 expression in wild-type tissues was compared with *bgh* mutant and knockout tissues.

3.3 Sperm and tissue staining

SPEF2 expression was studied with KAD antibody in testis sections, sperm samples, trachea, and kidney. Acetylated α-tubulin was used as a marker for microtubules of the ciliary axoneme. KAD antibody detected SPEF2 in seminiferous tubules at different stages of spermatogenesis. SPEF2 was localized to elongating spermatids, late spermatocytes, and Sertoli cells. In elongating spermatids, staining was observed in midpiece and tail (Figure 9).

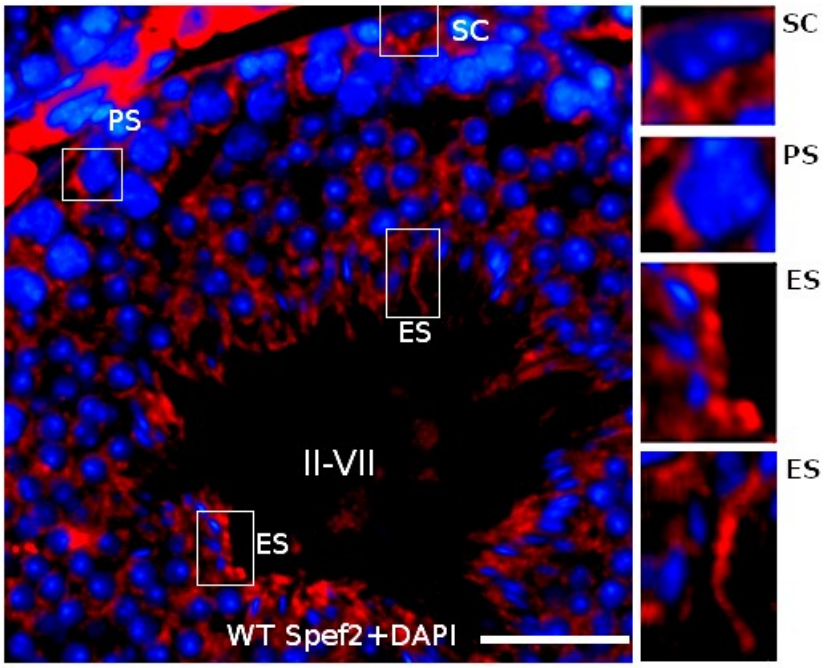

Figure 9. Spef2 expression in wild-type mouse testis. ES, elongating spermatids; PS, late spermatocytes; SC, Sertoli cell. SPEF2, *red*, DAPI, *blue*. Scale bar 20 µm.

Mature spermatids were present in lumina of seminiferous tubules. SPEF2 staining was more intense at stage II-VII tubules and weaker at stage IX-XI tubule. At stages IX-X, only step 9-10 spermatids are present. Therefore no midpiece or tail staining was observed in stage IX-XI tubule (Figure 10A-C). Late spermatocytes were stained (10C, insert). At stages II-VII, strong signal was detected in elongating spermatids (10D-F, insert). Heterozygote testis had normal appearance compared to wild-type testis. Elongating spermatids were observed and SPEF2 staining was comparable to wild-type (10G-I) Signal was also detected in round spermatids (Figure 10I, insert).

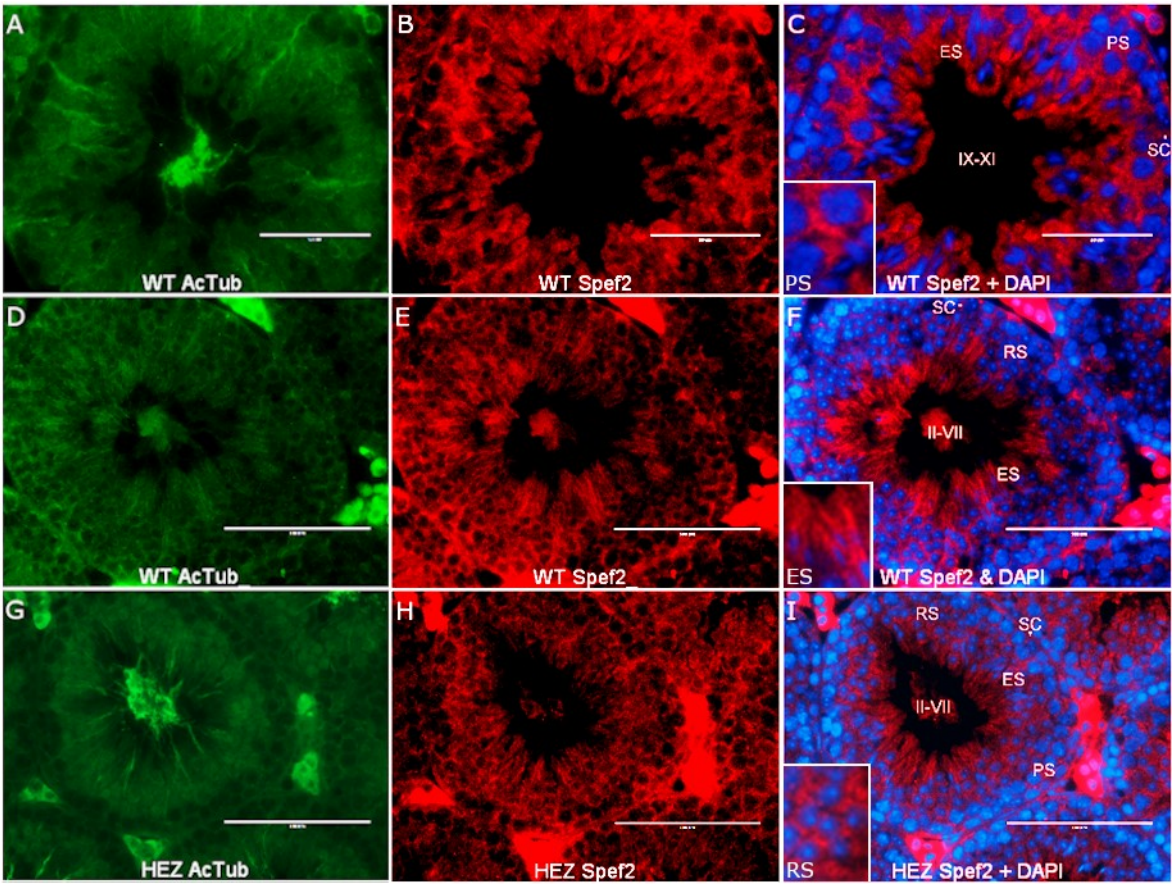

Figure 10. Spef2 expression in wild-type (WT) and heterozygote (HEZ) mouse testis during spermatogenesis. (A-C) Wild-type testis, stages IX-XI. (D-F) Wild-type testis, stages II-VII. (G-I) Heterozygote testis, stages II-VII). ES, elongating spermatids; RS, round spermatids; PS, late spermatocytes; SC, Sertoli cells. Acetylated α-tubulin, *green*, SPEF2, *red*, DAPI, *blue*.

Spermatid sample was prepared from a segment of mouse seminiferous tubule. In step 9–12 elongating spermatids, SPEF2 localized to manchette (Figure 11A-C). Mature spermatozoa were received from epididymis sample. KAD antibody stained specifically the midpiece of spermatozoa (Figure 11D-F). Acetylated α-tubulin stained microtubules in the manchette and sperm tail.

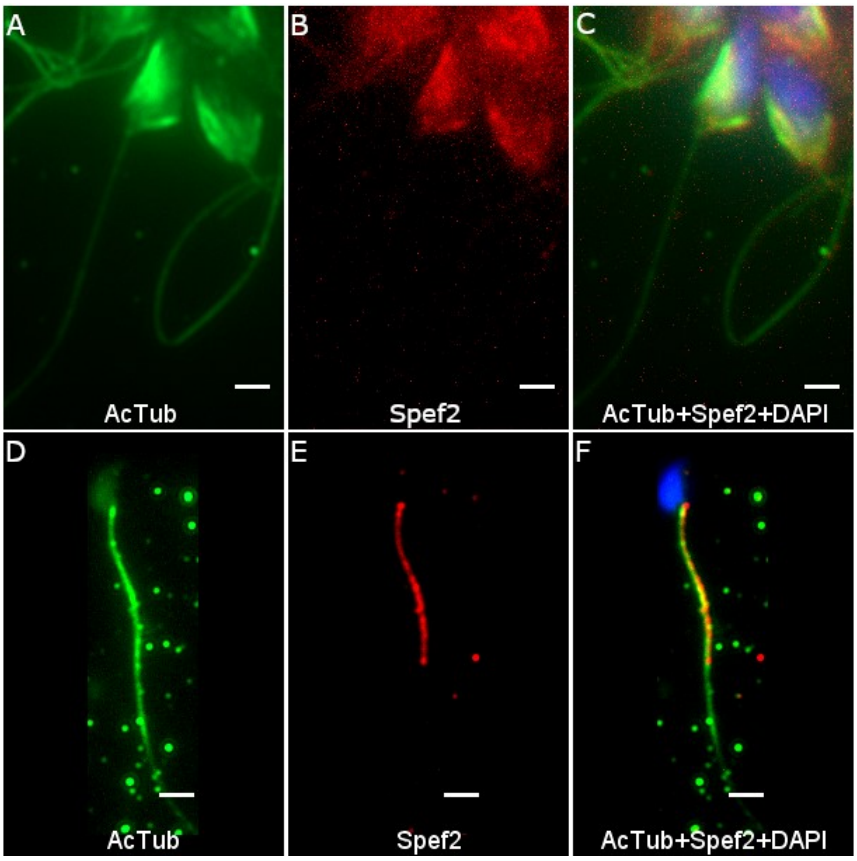

Figure 11. Spef2 expression in wild-type elongating spermatids and spermatozoa. (A-C) Manchette staining in step 9-12 spermatids. (D-E) SPEF2 stained midpiece in spermatozoa. AcTub, acetylated α-tubulin, *green*. SPEF2, *red.* Nuclear staining, DAPI, *blue*. Scale bar 5 µm.

Specific SPEF2 staining was detected in epithelial cilia in wild-type trachea (Figure 12A-C). In knockout trachea, staining was decreased. Acetylated α-tubulin indicated presence of the cilia in knockout trachea (Figure 12D-F). In kidney sections, SPEF2 staining appeared unspecific (Figure 13). Homozygote kidney tissue displayed normal tubule structure without cysts (Figure 13C-D).

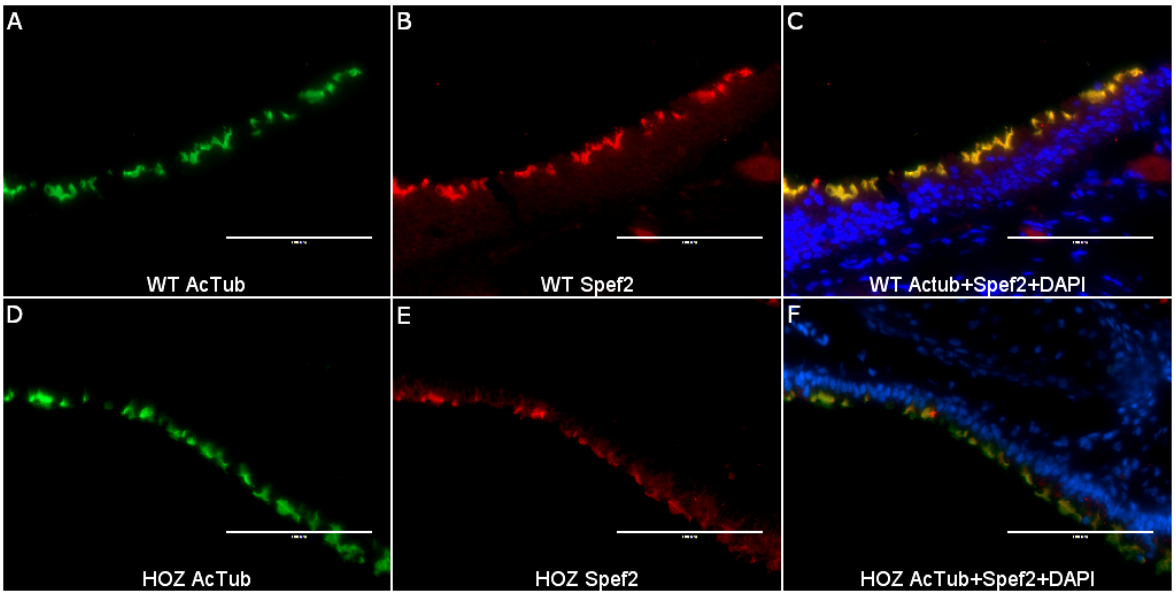

Figure 12. SPEF2 expression in wild-type and homozygous knockout mouse (HOZ) trachea. (A-C) Cilia staining in wild-type tracheal epithelial cells. (D-F) Cilia staining in knockout epithelial cells. AcTub, acetylated α-tubulin, *green*. SPEF2, *red*. Nuclear staining, DAPI, *blue*. Scale bar 100 µm.

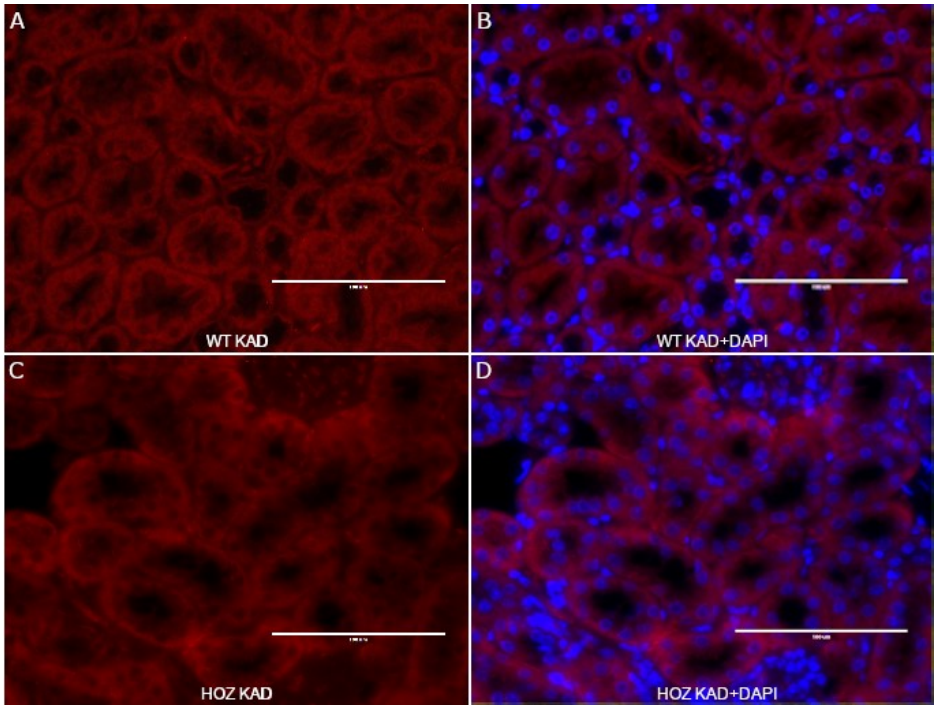

Figure 13. SPEF2 staining with KAD antibody in kidney tissues. (A-B) Kidney tubules of wild-type mouse. (C-D) Kidney tubules of a homozygous knockout mouse (HOZ). SPEF2, *red.* Nuclear staining, DAPI, *blue*. Scale bar 100 µm.

3.4 mIMCD3 cells

Three mIMCD3 cell lines were created for localization experiments. Each line was transfected with different SPEF2-GFP construct to express fusion proteins. 5'TE-GFP, KAD-GFP and 3'TE-GFP represent sequences of mouse testis-specific SPEF2-004 isoform (Figure 14A). 5'TE-fragment corresponds to N-terminus, KAD represents adenylate kinase domain, and 3'TE-GFP corresponds to C-terminus of SPEF2 protein. Acetylated α-tubulin was used as cilia marker and γ-tubulin as centrosomal marker. Fusion proteins were stained with anti-GFP antibody to amplify signal compared to GFP autofluorescence. GFP antibody was visualized in red channel with Alexa Fluor 555-secondary antibody.

5'TE-GFP was localized to basal body (14B) and cilia (14C). KAD-GFP localized to the basal body (14F), postmitotic spindle (14E), and centrosome (14G). 3'TE-GFP localized to cilia (14H), centrosome, and also extracentrosomal localization was detected (14I). In 5'TE-GFP-transfected cells, anti-SPEF2 antibody (anti-FLJ, Abnova) was tested. Abnova antibody binds to N-terminus of SPEF2 protein, and should recognize the 5´TE construct (14D). When cells were transfected with SPEF2-GFP constructs, GFP signal was punctuate due to localization to the cilia or cilia-associated structures. This indicated specificity of the GFP detection. In control with only GFP-containing plasmid, staining was dispersed in cytoplasm (14J-K), whereas GFP signal was missing in negative controls (14L-M).

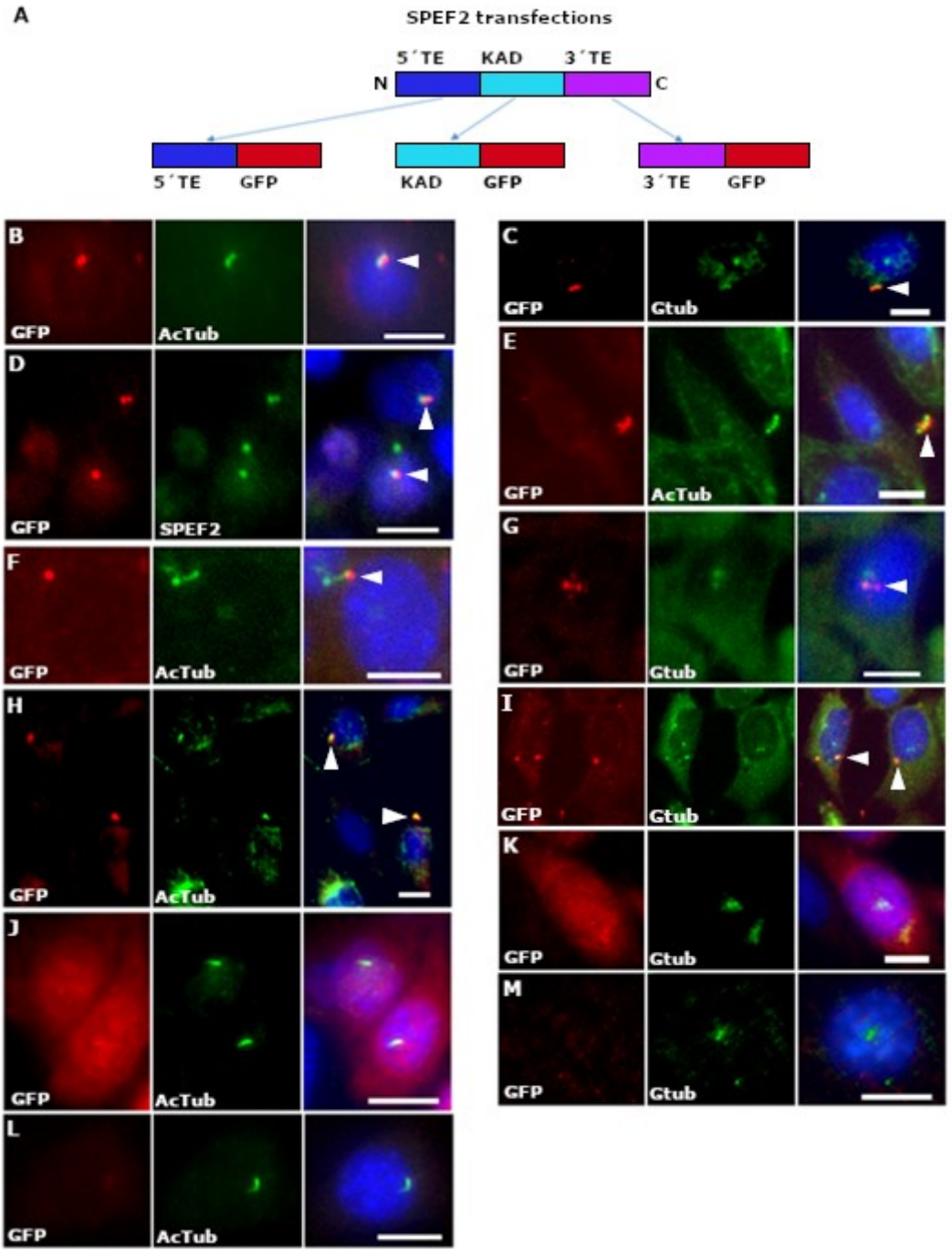

Figure 14.(A) mIMCD3 cell line was transfected with SPEF2-GFP fragments. (B-D) Cells transfected with 5'TE-GFP. (E-G) Cells transfected with KAD-GFP. (H-I) Cells transfected with 3'TE-GFP. (J-K) GFP-transfected controls. (L-M) negative control without transfection. AcTub, acetylated α-tubulin, *green*. SPEF2, *green,*was used in (D). Gtub, γ-tubulin, *green*. GFP, *red.* Nuclear staining, DAPI, *blue*. Colocalization of tubulins and SPEF2-GFP (arrowheads) is presented *yellow*. Scale bar 10 μm in B-E, H-M, 5 μm in F-G.

Transfection efficiency was measured by Fluorescence-activated cell sorter (FACS). Transfection percents were low, ranging from 7% to 12%, but comparable to positive transfection control (GFP). In negative control, 0,22% cells were recognized by cell sorter (Figure 15).

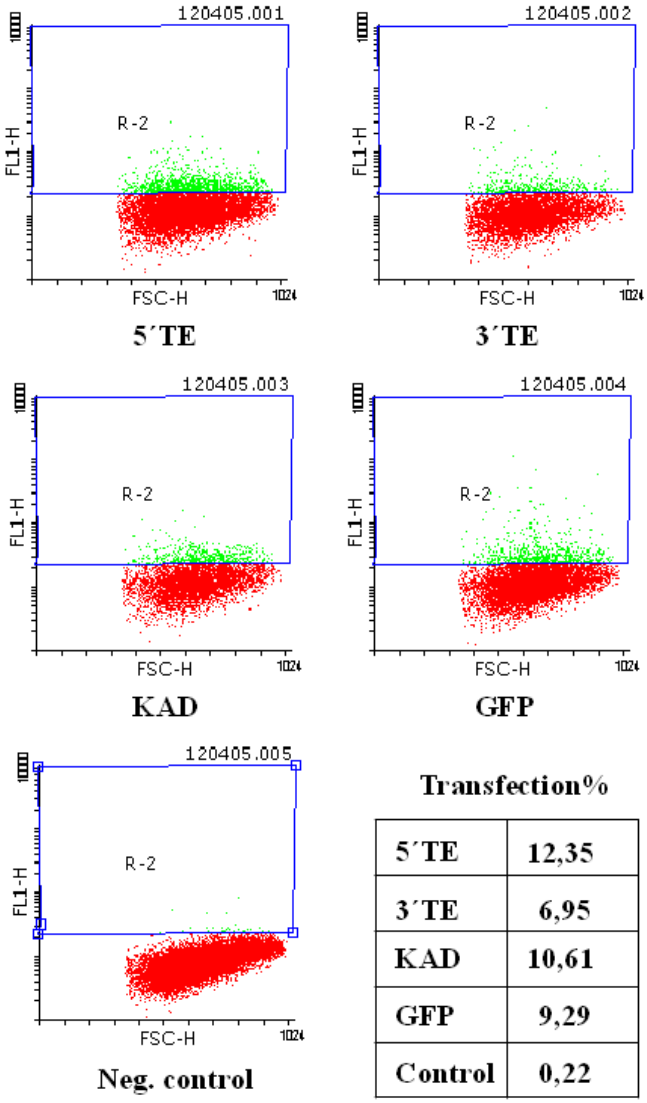

Transfection%

5´TE	12,35
3´TE	6,95
KAD	10,61
GFP	9,29
Control	0,22

Figure 15. Transfection efficiency was measured by fluorescence-activated cell sorter.

4 DISCUSSION

4.1 Novel SPEF2 antibody localizes in male germ cells and tracheal cilia

4.1.1 Production of SPEF2 antibody

Specificity of SPEF2 antibody was a challenge in this study. Low specificity was observed in both Western blot, and immunofluorescence experiments. Specificity is affected for example by quality of purified target antigen, or experiment protocols and conditions. In case of *Spef2* KO mice, also presence of the real target antigen in KO tissues is possible. In KO mice, *Spef2* gene lacks only exons 3-5, whereas antibody target domain is located to later exons. SPEF2 has multiple isoforms, and the antibody might bind to some of the shorter isoforms.

Novel SPEF2 antibody is polyclonal. Polyclonal antibodies bind to multiple antigenic determinants of the target, and they have an ability to recognize antigens, when target´s tertiary stucture is changed. On the other hand, this can cause higher cross-reactivity (Ascoli and Aggeler 2018). Preparation of antigen is a critical step in polyclonal antibody production. Impurities of antigen can cause the host animal to produce antibodies targeted to impurities, instead of desired target. Presence of bacterial antigens, such as E. coli cell debris, affects the specificity (Leenaars and Hendriksen 2005).

Yield of SPEF2 antigen in chromatography was low. For new recombinant proteins, cultivation and purification protocol might require individual optimization. Cultivation conditions of E. coli, efficacy of lysis buffer, and fusion protein solubility can affect the yield. Antigen production and yield could be improved by cultivation in lower expression temperature, which can reduce protein aggregation and degradation. Cell density, composition of cell growth medium, and inducer concentration could be further adjusted (Costa et al. 2014).

4.1.2 SPEF2 is detected in sperm, testis and trachea in immunofluorescence staining

Novel SPEF2 antibody was used to detect SPEF2 expression in sperm and testis by immunofluorescence staining. In sperm slides, SPEF2 was expressed in the middle piece of mature spermatozoa. In male germ cell preparation from the testis, SPEF2 was localized to manchette of elongating spermatids. SPEF2 staining localized to elongating spermatids, round spermatids, late spermatocytes, and Sertoli cells in the testis. Function of SPEF2 in Sertoli cells remains yet unknown (Sironen et al. 2010).

Specificity of the novel SPEF2 antibody was supported by spermatid staining during spermatogenesis. Sironen et al. (2010) utilize antibody targeted to C-terminal domain of SPEF2, which demonstrates manchette and midpiece staining. As long SPEF2 isoform is expressed in sperm and testis, antibody binding to KAD domain was predicted to detect similar expression pattern as C-terminal antibody. Prediction was confirmed in WT testis sections. However, sections had unspecific staining in Leydig cells at interstitial space adjacent to seminiferous tubules. Unspecific Leydig cell staining in the testis is not uncommon (McAnich et al. 2020). SPEF2 staining with KAD antibody is absent in knockout testis, which indicates that

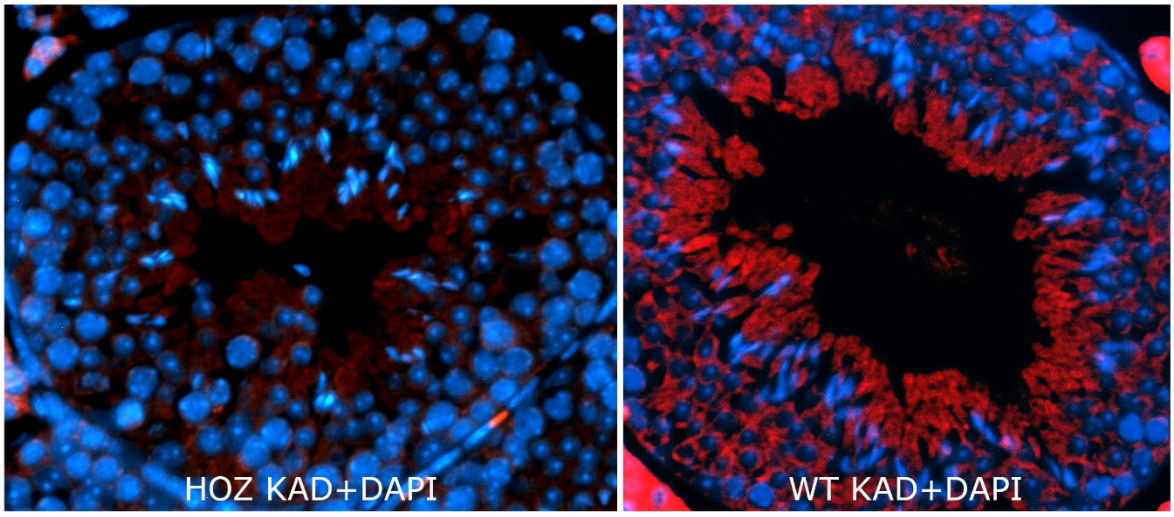

Figure 16. KAD antibody staining (*red*) in homozygous knockout (HOZ) testis and wild-type (WT) testis. SPEF2 staining is absent in knockout testis. (Photo courtesy of Mari Lehti.)

the antibody specifically recognizes SPEF2 isoforms expressed in the testis (Figure 16, Lehti et al., unpublished data).

SPEF2 was localized to cilia in wild-type and KO trachea, and staining was decreased in KO tissue. SPEF2 signal in KO trachea could be caused by unspecific staining or presence of short SPEF2 isoforms in the tissue. In KO trachea, the cilia were visible with acetylated α-tubulin. It appears that absence of full-length SPEF2 does not prevent cilia formation in trachea. Cilia were not clearly distinguished in WT or KO kidneys with SPEF2 antibody. Kidney epithelial cells contain only one cilia. Cilia could be visualized with higher magnification imaging. Possibly SPEF2 expression in the kidney is too low to be detected with SPEF2 antibody.

Fixing method and antigen retrieval can affect staining. Cryosections maintain antigens better than paraffin sections. Protocol optimization, such as detergent use and washes, may reduce unspecific background. Kidney sections are more challenging to stain than cell culture, since cilia are not uniformly oriented in tissue. Each cross section might not contain multiple cilia (Deane et al. 2012).

4.2 SPEF2 has tissue-specific isoforms and several ciliary localization sequences

4.2.1 Spef2 isoforms in Western blot

Expression of full-length SPEF2 ~250 kDa was observed in testis tissue from 2 weeks age throughout spermatogenesis, and also in adult epididymis. Isoform ~200 kDa was present only in testis (Figure 8A). In the mouse, SPEF2 has six protein coding sequences reported at Ensembl database (Figure 6). Molecular weights observed in Western blot correspond to transcripts **SPEF2-006** and **SPEF2-004**, respectively. Sources of ~200 kDa isoform could be spermatocytes, spermatids, and Sertoli cells. Possible function of ~200 kDa isoform could be intramanchette transport in spermatids, which partially differs from intraflagellar transport in cilia. Epididymis contains only mature spermatozoa. Specificity of the SPEF2 antibody is supported

by absence of long isoforms of ~250 kDa and ~200 kDa in testis lysates of *bgh* mutant and two KO males (Figure 8B). Presence of full-length SPEF2 in lung and oviduct indicates, that this isoform is involved in ciliary motility in multiciliated epithelial cells in addition to sperm flagella. ~100 kDa band was observed in both WT and KO tissues (Figure 8B). Isoforms SPEF2-001 has predicted weight ~100 kDa, but according Ensembl, this isoform contains exons 1-3. SPEF2 KO mouse lacks exons 3-5, which indicates that ~100 kDa band is unspesific. None of the clear bands corresponded isoforms SPEF2-002, SPEF2-003, and SPEF2-005, which have predicted molecular weight approx. 50-70 kDa.

Previous studies of SPEF2 present Western Blots of porcine, mouse and bovine tissues. In porcine testis, besides the long isoform, two shorter isoforms of approximately 110 kDa and 125 kDa are expressed (Sironen et al. 2010). In Holstein bulls, two proteins ~200 and 190 kDa have been observed in Western blot of testis samples. For the bulls, predicted molecular weights of the SPEF2-complete and SPEF2-alternative splicing are 202 and 195 kDa, respectively (Guo et al. 2014). These data support findings in this study, that at least two isoforms of SPEF2 protein are present in testis, although differences across species occur. Recent Western blot analyses of human samples reveal ~200 kDa band in sperm (Liu et al. 2019), and ~210 kDa band in primary respiratory cell cultures (Cindric et al. 2020). Mouse samples in this study showed similar expression pattern, as single >200 kDa bands were observed in epididymal sperm and lung tissue. SPEF2 antibodies have been raised against different binding sites, and use of different antibody may affect results. Short SPEF2 isoforms may lack exons at N- or C-terminus of full-length protein and remain undetected. Western blot appears reliable method for detecting long SPEF2 isoforms.

Low expression may be unnoticed in gel analysis, due to low resolution of Western blot. Differences in exons might not differ in molecular weight. KAD antibody recognized full-length protein from the postnatal day 14 (PND14). Shorter isoform of SPEF2 mRNA is detected in wild-type testis at PND7, when first wave of

spermatogenesis has been initiated. SPEF2 mRNA is expressed in round spermatids. Round spermatids appear at PND21, which increases SPEF2 expression (Sironen et al. 2010). Long SPEF2 isoform in the lung was detected in this study. Based on previous mRNA studies, exon 6 may be missing in the lung isoform (Sironen et al. 2010). This difference would not be visible in Western blot. Possible brain-specific ~120 kDa isoform was detected with KAD antibody, and also mRNA study recognizes shorter isoform in the brain. Ependymal cilia create flow of cerebrospinal fluid in the brain, and immotily of these cilia is likely to result gross hydrocephalus observed in *bgh* mutant mice (Sironen et al. 2011). Hydrocephalus is also present in other *Spef2* KO strains, but its severity varies (Table 2). RNA-Seq is a sensitive method and takes account expression of all exons. The RNAseq data from Laiho et al. (2013) was used to quantify Spef2 transcripts in the mouse testis during the first wave of spermatogenesis (Figure 17). Expression rapidly increases after postnatal day 17, at which point SPEF2 is already detected in Western blot.

SPEF2 expression has been analyzed from wild-type mouse tissues at mRNA level. In PCR, fragment spanning from exons 6 to 43 is predominantly expressed in the

	PND7	PND14	PND17	PND21	PND28
Spef2	0,031499	5,55911	7,74442	15,1045	24,4999

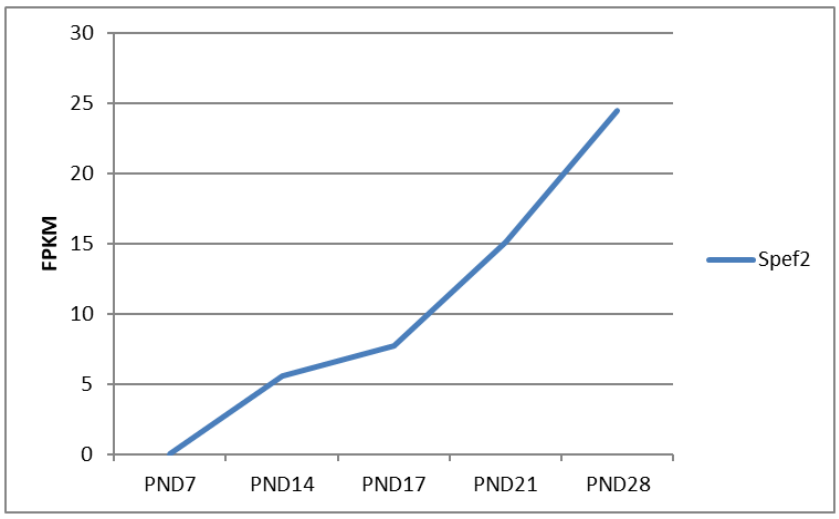

Figure 17. *Spef2* gene expression in mouse testis, from postnatal day 7 to postnatal day 28. RNA-seq data is announced in FPKM units (fragments per kilobase of exon model per million reads mapped). (Laiho et al. 2013). (Figure courtesy of Anu Sironen.)

testis, whereas the shorter fragments covering the exons 3-7 and 37-43 are expressed in the lung, brain, kidney, and liver. Also mRNA lacks exon 4 in these tissues (Sironen et al. 2010). It is possible that N-terminal or C-terminal part has a more general role in cilia development. SPEF2 contains putative NLS that contain basic amino acid residues and fit the consensus sequence of a bipartite NLS. One of these occurs at residues 238-255, the other two overlap at residues 1217-1234 and 1224-1241 (Ostrowski et al. 1999).

Western blot experiments contained extra bands and smeared bands. Unusual or unexpected bands can be caused by digested target proteins. High background is often caused by too high concentration of the antibody. Antibody concentration could be decreased, and run a control with secondary antibody without the primary. Non-specific bands can be distinguished using blocking peptides. When antibody is incubated with peptide, only specific band are blocked and thus disappear (Mahmood and Yang 2012, Pillai-Kastoori et al. 2019). Protein identity should be verified with complementary technique, such as mass spectrometry. Protein bands can be extracted from polyacrylamide gel and analyzed with MALDI-TOF (matrix-assisted laser desorption/ionization-time of flight) mass spectrometry (Fernandez et al. 1998).

4.2.2 SPEF2 localizes to basal body, cilium, and centrosome in mIMCD3 cells

Three SPEF2-GFP fusion proteins were expressed in mIMCD3 cell line to study ciliary transport of different domains. Ciliary proteins contain a ciliary localization sequence (CLS). Work hypothesis was that N-terminal fragment (5´TE) or KAD fragment would contain a CLS. Functional SPEF2 N-terminus is required for manchette function and tail formation (Lehti et al. 2017). C-terminal part of the SPEF2 protein sequence (amino acids 1577-1812 in porcine sequence) is not present in Chlamydomonas rheinhardtii homologue, CPC1. Thus SPEF2 is likely to have CLS in conserved part, either N-terminal domain, or close to adenylate kinase domain. This study suggests, that also C-terminal part (3´TE) could contain CLS.

For colocalization studies, centrosomes were stained with ɤ -tubulin, and cilia were labeled with acetylated α-tubulin. ɤ -tubulin, a member of tubulin superfamily required for microtubule nucleation, is associated with centrosome throughout the vertebrate cell cycle. In postmitotic ciliated cells, the major microtubule organizing centers are the basal bodies that provide template for the ciliary axonemes. ɤ-tubulin localizes at the basal body regions. Acetylated α-tubulin localizes to ciliary axoneme. Acetylation of α-tubulin of was first reported by L'Hernault and Rosenbaum (1983), who observed that the α-tubulin in flagella was posttranslationally modified and mapped it to the ε-amino group of a single lysine residue. Acetylation stabilizes microtubules to form cilia, and deacetylation occurs when cilia are resorbed. Colocalization with tubulins places SPEF2 to basal body, cilium and centrosome. Control plasmid for GFP expression was used to measure transfection efficiency. In control cells, GFP expression was evenly dispersed in the cytoplasm, whereas in SPEF2 transfected cells GFP expression was punctuate. 5´TE, KAD and 3´TE sequences were all sufficient for SPEF2 localization to the cilium or basal body. Weakness in these experiments was the use of red secondary antibody. Fluorescence of GFP itself was considered too weak to detect punctuate expression, thus the cells were stained with anti-GFP. However, there is a possibility that fluorescence emission of GFP can interfere with the localizations of the tubulins stained with green secondary antibody.

Ciliary proteins are transported through the cytoplasm to the cilium base, where they are translocated to ciliary shaft by intraflagellar transport. CLSs are diverse, which suggests that they interact with different pieces of the transport machinery. VxP motif is characteristic for transmembrane and membrane-associated proteins. CLSs of cytoplasmic proteins are less well characterized (Malicki and Avidor-Reiss 2014). IFT20 appears to facilitate cilia-directed trafficking in the cytoplasm, and is localized also in the Golgi complex with SPEF2. IFT20 may contribute to transport of SPEF2 to the basal body and cilium (Sironen et al. 2010).

Ciliary localization signals share similarities with nuclear localization signals (NLS) (Malicki and Avidor-Reiss 2014). One example of cytoplasmic ciliary-targeted protein is Kinesin-like protein 17 (Kif17) Ciliary targeting sequence of Kif17 is related to NLS, and located in the C-terminus of the protein. Interestingly, Kif17 C-terminal domain alone localizes to nucleus. This suggests that similar mechanisms may control nuclear and ciliary targeting (Dishinger et al. 2010). Occasionally, a protein can contain multiple CLSs. Retinitis pigmentosa 2 protein (RP2) contains two sequences independently sufficient to ciliary localization facilitated by Importin β2 (Hurd et al. 2011). Splicing variants of SPEF2 might contain different CLSs.

Transfection efficiency in mIMCD3 cells was low, even though lipofection is often considered method of choice. For stable transfection, genetic materials that have a marker gene for selection (transgenes) are integrated into the host genome and sustain transgene expression even after host cells replicate. Transiently transfected genes are expressed for a limited period of time and are not integrated into the genome. Of chemical methods, cationic lipids are a common method. Nucleic acid/chemical complex pass the cell membrane by endocytosis or phagocytosis. Transfection efficiency of chemical methods is dependent on factors such as nucleic acid/chemical ratio, solution pH, cell membrane conditions, and the cell type. The process results in low transfection efficiency compared to virus-mediated methods. Advantages of lipofection include low cytotoxicity, no mutagenesis, and no size limitation on the packaged nucleic acid (Kaestner et al. 2015, Palchetti et al. 2017). Antibiotic selection is a commonly used method in cell cultures. An alternative method to enrich desired cell population is fluorescence-based sorting (Palchetti et al. 2017). In this study, geneticin was used as a selective agent. Different antibiotic selection could be an option to improve transfection efficiency.

4.3 *Spef2* knockout mice and PCD phenotype

Spef2 KO mouse is a model for primary ciliary dyskinesia. Hydrocephalus in *Spef2* KO mice is severe enough to cause postnatal lethality (Figure 18). PCD phenotype is only observed in homozygous individuals. Thereby one copy of *Spef2* gene is sufficient to formation and function of the cilia. KO mice display situs solitus, which implies that embryonic nodal cilia are not affected by *Spef2* mutation. *Spef2* full KO lacks all N-terminal isoforms (Lehti et al. 2018).

Figure 18. *Spef2* knockout mice have severe hydrocephalus and grow retardation. (Photo courtesy of Anu Sironen.)

Spef2 KO mice suffer from growth retardation, and most die before reaching sexual maturity. Osteoblasts and chondrocytes have primary cilia, and SPEF2 is expressed in developing bone and cartilage. In *Spef2* KO mice, osteoblast differentiation is impaired, which leads to defective bone formation. Absence of long SPEF2 isoforms leade to multiple morphological abnormalities of the sperm flagella (MMAF) phenotype. Bone phenotype is probably caused by absence of shorter N-terminal isoform (Lehti et al. 2018). However, in this study appearance of KO kidneys did not differ from WT tissue. There are no data, whether knocking out Spef2 has minor effects in the kidney, or if symptoms develop later in age. Kidney cysts are observed in many ciliopathies, but rarely in primary ciliary dyskinesia (Horani and Ferkol 2016). Polycystic kidney disease mouse models develop numerous tubular and

glomerular cysts, epithelial hyperplasia and inflammation in the kidneys (Kurbegovic and Trudel 2013).

In osteoblasts and chondrocytes, signaling and IFT in primary cilia may differ from the functions in renal cilia. Different mutations in the same gene can affect protein production in multiple organs correlating with disease severity. For example, mutations in *centrosomal protein of 290 kDa (CEP290)* are associated with several ciliopathies. *CEP290* mutations cause Leber congenital amaurosis, Senior-Löken, Joubert, and Meckel-Gruber syndrome. Leber congenital amaurosis affects only eyes, whereas Meckel-Gruber syndrome is pre- or postnatally lethal (Drivas et al. 2015). Joubert syndrome is genetically and phenotypically heterogenic. Universal features in Joubert syndrome are brain malformations developmental delay, ataxia and apnea. Variable symptoms may affect skeleton, kidney tissue, or both, depending on causative mutation. Joubert subtyoes include renal cysts, polydactyty and skeletal dysplasias (Parisi 2019).

Gross hydrocephalus resulting from *Spef2* mutation has been previously observed in *bgh* mice (Table 2). Dysfunction of ependymal cilia and abnormal cilia-driven flow are important factors, but might not be the sole determinant of the severity of hydrocephalus. In *bgh* mice, hydrocephalus is severe in mice with C57BL/6J background compared to 129S6/SvEvTac mice. In mutants with B6 background, there is ependymal sloughing and loss of cilia along the surface of lateral ventricles, ventricular dilatation and white matter damage. These mouse models suggest that severe congenital hydrocephalus is generally influenced by genetic modifiers (Finn et al. 2014). Bone formation has not been examined in *bgh* mutant.

Tu et al. (2020) present *Spef2* KO mouse model that lacks exons 3-6 (Table 2). About 20% of mice, with milder form of hydrocephalus, survive to sexual maturity. Longer lifespan makes available to observe effects of SPEF2 absence on both somatic and germ cells. Besides male infertility, females are subfertile. Beat frequency of oviduct cilia is reduced (Tu et al. 2020). To date, respiratory cilia have been studied in *bgh*

and *Spef2* KO mice lacking exons 3-6. Both mice have normal ultrastructure of tracheal epithelial cilia, but cilia show reduced beat frequency and mice develop sinusitis (Sironen et al. 2011, Tu et al. 2020). Male germ cell-specific conditional KO mouse is generated for spermatogenesis research. In cKO mice, absence of N-terminal domain of SPEF2 impairs manchette function and tail formation, and leads to multiple morphological abnormalities of the sperm flagella (MMAF) phenotype (Lehti et al. 2017).

Recently, *Spef2* mutations have been described also in patients with MMAF. Tu et al. (2020) report six affected males in four Chinese families. Homozygous *Spef2* mutation is identified as a cause of MMAF. Observed symptoms of the six SPEF2-associated MMAF patients resemble phenotype of *Spef2* KO mouse strains. Symptoms in patients include chronic respiratory infections with normal ultrastucture in cilia, but irregular or slow beating, otitis, male infertility resulting from various sperm defects, and in one case, female infertility. Patients have situs solitus. Mutations in these patiens localize to the middle of *Spef2* gene, between adenylate kinase domain and IFT20 binding domain. Neither of the patients had other PCD_related symptoms, such as respiratory infections. Sha et al. (2019) report MMAF patient with biallelic mutations in the *Spef2* gene. Other mutation results in a truncated protein missing the IFT20-binding domain and the entire C-terminus, and the other mutation presents premature Stop codon after IFT20 binding sequence. The patient did not suffer from other PCD-related symptoms, and chest X-ray shows normal development of the chest.

Regardless of position in the gene, homozygous or biallelic *Spef2* mutations resulted in MMAF phenotype in mice, pigs and humans. Thereby full-length protein is crucial to sperm development. Germ-cell specific phenotype was observed in pigs and humans, when the mutation is located at the 3´end of the *Spef2* gene. In humans, mutations in the middle exons of *Spef2* appear to cause airway diseases in addition to male infertility. Mutations affecting only N- or C-terminus of SPEF2 protein may allow expression of shorter variants, which could rescue motility in human

respiratory epithelial cells. In mice, absence of N-terminal part of SPEF2 causes airway disease in two mouse strains. Absence of SPEF2 in oviduct can decrease female fertility in humans and mice, but effect is not as clear.

4.4 Future prospects

Ciliopathies are traditionally classified as diseases of motile cilia, or non-motile primary cilia. Some mutations can cause defects in both cilia types. IFT mutations cause variety of phenotypes. Disruption in IFT causes cilia loss in osteoblasts, such as deletion of IFT20. Skeletal abnormalities in *Spef2* KO mouse models point out, that SPEF2 can function in primary cilia. Whether SPEF2 has active role in other cell types with sensory cilia, is a subject of future research. In addition to epithelial kidney cells in this study, *Spef2* could be transfected into another ciliated cell line to observe its role in primary cilia. Expression of ciliopathy genes, such as polycystins, has been investigated in osteoblast and osteocyte cultures (Xiao et al. 2006).

Few interacting partners of SPEF2 have been identified: HYDIN (Cindric et al. 2020), IFT20, dynein 1, and GOLGA3 (Lehti et al. 2017). Interaction with proteins localized to Golgi apparatus or cytoplasm suggest, that SPEF2 might have a role in vesicular transport from Golgi to the cilium (Lehti et al. 2017). Localization of SPEF2 has been described in detail in male germ cells and mature spermatozoa. In cell models, possible localization to Golgi and transport to cilium could be visualized by live cell imaging. Interacting proteins have been identified by co-immunoprecipitation (co-IP) of testis extracts. co-IP could reveal interactions in other tissues, such as ependymal cilia in the brain, where a shorter isoform of SPEF2 is expressed. Pull down assays in ciliated cell lines like mIMCD might detect physical interactions between proteins. Specific interaction constructs, such as gene silencing of interacting partners (e.g. IFT20) could be utilized to identify transport mechanisms.

Compared to sperm flagella, structure and organization in motile cilia are not drastically affected by *Spef2* mutations. Diagnostic methods of PCD have

limitations. Female patients might be fertile, or the cause of their infertility can be hard to identify. Electron microscopy of respiratory cilia can be inconclusive in case of central pair-affecting mutations with minor structural changes. Ciliary beat is evaluated by videomicroscopy of nasal brush biopsy. High-speed video microscopy analysis (HSVA) is considered as sensitive and specific method to classify disease as PCD (Rubbo et al. 2019).

Recent findings of *Spef2* mutations in humans have concentrated mainly on Chinese population. In mice, genetic background affects severity of PCD caused by *Spef2* depletion. It remains to be seen, which factors affect phenotype in humans. Prevalence of *Spef2* mutations in other populations is yet unknown. Incidence rate could determine, whether it is profitable to screen patients for *Spef2* mutations. Progressive damage to respiratory system, bronchiectasis, has been observed in patients with SPEF2-associated PCD. In future, if *Spef2* mutations were identified in youth, early and specific treatment of respiratory illness could improve prognosis.

5 CONCLUSIONS

In this study, a novel antibody was developed against adenylate kinase domain of SPEF2. Multiple SPEF2 variants have been identified at mRNA or protein level in previous research. SPEF2 variants are expressed in a tissue-specific manner. Novel antibody was utilized in Western blot and immunofluorescence stainings. SPEF2 isoforms were detected in WT mouse sperm, testis, epididymis, lung, oviduct, and brain. Specificity of the antibody was a challenge in both techniques, and protocols require further optimization. Antibody was most reliable in sperm, testis and trachea samples, where SPEF2 expression level is highest. Identity of proteins should be confirmed with complementary technique, preferably mass spectrometry.

Tissue samples of *Spef2* KO and *big giant head* mice were examined in this study. Spermatogenesis and ciliary motility are defective in PCD mouse models. In *bgh* and KO mice, long SPEF2 isoforms were absent in the testis. Mouse phenotypes indicate that correct SPEF2 expression and localization to the cilia is essential at least in the testis, trachea, and brain. Previous research points out, that SPEF2 is associated with proteins, which localize to central pair microtubules in motile cilia, and Golgi apparatus. These data emphasize role of SPEF2 in ciliary motility rather than in sensory cilia. Interestingly, SPEF2 affects bone formation in full KO. This indicates that SPEF2 participates in some basic ciliary functions required in motile as well as immotile cilia.

SPEF2 fusion proteins were expressed in mIMCD3 cell line. Transfections demonstrated, that SPEF2 localizes to the cilia also in other cell types that male germ cells. Three separate domains of SPEF2 were able to facilitate its transport to the basal body and cilium. Results suggest, that SPEF2 contains multiple ciliary localization signals to ensure transport of shorter isoforms to the cilia. Cell models could further elucidate function of SPEF2 isoforms in somatic cells.

ACKNOWLEDGEMENTS

This Master's thesis was accomplished at LUKE, Natural Resources Institute Finland.

First of all I want to thank my instructor Anu Sironen for giving me oppoturnity to do this research. I want to thank you for your guidance and support. Thanks to professor Johanna Vilkki and senior scientist Maria Tuiskula-Haavisto for letting me to work at your department of Animal Genomics. Special thanks for materials and technical assistance to Mari Lehti and Mervi Mutikainen.

REFERENCES

Andersson M., Peltoniemi O., Makinen A., Sukura A. & Rodriguez-Martinez H. 2000. The hereditary 'Short tail' sperm defect - A new reproductive problem in yorkshire boars. *Reproduction in Domestic Animals* 35: 59–63.

Anvarian Z., Mykytyn K., Mukhopadhyay S., Pedersen L. B. & Christensen S. T. 2019. Cellular signalling by primary cilia in development, organ function and disease. *Nat Rev Nephrol* 15: 199-219.

Ascoli C.A. & Aggeler B. 2018. Overlooked benefits of using polyclonal antibodies. *BioTechniques* 65: 127-136.

Besschetnova T.Y., Roy B. & Shah J.V. 2009. Imaging intraflagellar transport in mammalian primary cilia. *Methods Cell Biol* 93: 331-346.

Borg C.L., Wolski K.M., Gibbs G.M. & O'Bryan M.K. 2010. Phenotyping male infertility in the mouse: how to get the most out of a 'non-performer'. *Hum Reprod Update* 16: 205-224.

Breslow D.K. & Holland A.J. 2019. Mechanism and Regulation of Centriole and Cilium Biogenesis. *Annu Rev Biochem* 88: 691-724.

Buffone M.G., Ijiri T.W., Cao W., Merdiushev T., Aghajanian H.K. & Gerton G.L. 2012. Heads or tails? Structural events and molecular mechanisms that promote mammalian sperm acrosomal exocytosis and motility. *Mol Reprod Dev* 79: 4-18.

Bujakowska K.M., Liu Q. & Pierce E.A. 2017. Photoreceptor Cilia and Retinal Ciliopathies. *Cold Spring Harb Perspect Biol* 9 (10), a028274, doi: 10.1101/cshperspect.a028274.

Cindric S., Dougherty G.W., Olbrich H., Hjeij R., Loges N.T., Amirav I., Philipsen M.C., Marthin J.K., Nielsen K.G., Sutharsan S., Raidt J., Werner C., Pennekamp P., Dworniczak B. & Omran H. 2020. SPEF2- and HYDIN-Mutant Cilia Lack the Central Pair-associated Protein SPEF2, Aiding Primary Ciliary Dyskinesia Diagnostics. *Am J Respir Cell Mol Biol* 62: 382-396.

Costa S., Almeida A., Castro A. & Domingues L. 2014. Fusion tags for protein solubility, purification and immunogenicity in Escherichia coli: the novel Fh8 system. *Front Microbiol* 5: 63. doi:10.3389/fmicb.2014.00063.

Deane J.A., Verghese E., Martelotto L.G., Cain J.E., Galtseva A., Rosenblum N.D., Watkins D.N. & Ricardo S.D. 2013. Visualizing renal primary cilia. *Nephrology (Carlton)* 18: 161-168.

Dishinger J.F., Kee H.L., Jenkins P.M., Fan S., Hurd T.W., Hammond J.W., Truong Y.N., Margolis B., Martens J.R. & Verhey K.J. 2010. Ciliary entry of the kinesin-2 motor KIF17 is regulated by importin-beta2 and RanGTP. *Nat Cell Biol* 12: 703-710.

Drivas T.G., Wojno A.P., Tucker B.A., Stone E.M. & Bennett J. 2015. Basal exon skipping and genetic pleiotropy: A predictive model of disease pathogenesis. *Sci Transl Med* 7: 291ra97. doi:10.1126/scitranslmed.aaa5370.

Dzeja P. & Terzic A. 2009. Adenylate kinase and AMP signaling networks: metabolic monitoring, signal communication and body energy sensing. *Int J Mol Sci* 10: 1729-1772.

Ensembl. (2020). (Accessed 10.11.2020). Mouse Spef2 transcripts. Gene: Spef2 (ENSMUSG00000072663) - Summary - Mus_musculus - Ensembl genome browser 102

Fernandez J., Gharahdaghi F. & Mische S.M. 1998. Routine identification of proteins from sodium dodecyl sulfate-polyacrylamide gel electrophoresis (SDS-PAGE) gels or polyvinyl difluoride membranes using matrix assisted laser desorption/ionization-time of flight-mass spectrometry (MALDI-TOF-MS). *Electrophoresis* 19: 1036-1045.

Finn R., Evans C.C. & Lee L. 2014. Strain-dependent brain defects in mouse models of primary ciliary dyskinesia with mutations in Pcdp1 and Spef2. *Neuroscience* 277: 552-567.

Fliegauf M., Benzing T. & Omran H. 2007. When cilia go bad: cilia defects and ciliopathies. *Nat Rev Mol Cell Biol* 8: 880-893.

Follit J.A., Tuft R.A., Fogarty K.E. & Pazour G.J. 2006. The intraflagellar transport protein IFT20 is associated with the Golgi complex and is required for cilia assembly. *Mol Biol Cell* 17: 3781-3792.

Franca L.R., Hess R.A., Dufour J.M., Hofmann M.C. & Griswold M.D. 2016. The Sertoli cell: one hundred fifty years of beauty and plasticity. *Andrology* 4: 189-212.

Girardet L., Augière C., Asselin M. P. & Belleannée C. (2019). Primary cilia: Biosensors of the male reproductive tract. Andrology 7: 588-602.

Guo F., Yang B., Ju Z.H., Wang X.G., Qi C., Zhang Y., Wang C.F., Liu H.D., Feng M.Y., Chen Y., Xu Y.X., Zhong J.F. & Huang J.M. 2013. Alternative splicing, promoter methylation, and functional SNPs of sperm flagella 2 gene in testis and mature spermatozoa of Holstein bulls. *Reproduction* 147: 241-252.

Harris P.C. & Torres V.E. 2009. Polycystic kidney disease. *Annu Rev Med* 60: 321-337.

Hermo L., Pelletier R.M., Cyr D.G. & Smith C.E. 2010. Surfing the wave, cycle, life history, and genes/proteins expressed by testicular germ cells. Part 1: background to spermatogenesis, spermatogonia, and spermatocytes. *Microsc Res Tech* 73: 241-278.

Hermo L., Pelletier R.M., Cyr D.G. & Smith C.E. 2010. Surfing the wave, cycle, life history, and genes/proteins expressed by testicular germ cells. Part 2: changes in spermatid organelles associated with development of spermatozoa. *Microsc Res Tech* 73: 279-319.

Hess R.A. & Renato de Franca L. 2008. Spermatogenesis and cycle of the seminiferous epithelium. *Adv Exp Med Biol* 636: 1-15.

Horani A. & Ferkol T.W. 2016. Primary ciliary dyskinesia and associated sensory ciliopathies. *Expert Rev Respir Med* 10: 569-576.

Hurd T.W., Fan S. & Margolis B.L. 2011. Localization of retinitis pigmentosa 2 to cilia is regulated by Importin beta2. *J Cell Sci* 124: 718-726.

Ishikawa T. 2017. Axoneme Structure from Motile Cilia. *Cold Spring Harb Perspect Biol* 9: a028076. doi: 10.1101/cshperspect.a028076.

Kaestner L., Scholz A. & Lipp P. 2015. Conceptual and technical aspects of transfection and gene delivery. *Bioorg Med Chem Lett* 25: 1171-1176.

Keeling J., Tsiokas L. & Maskey D. 2016. Cellular Mechanisms of Ciliary Length Control. *Cells* 5(1):6. doi:10.3390/cells5010006.

Kent T. & Griswold M.D. 2014. Checking the Pulse of Vitamin A Metabolism and Signaling during Mammalian Spermatogenesis. *J. Dev. Biol.* 2: 34-49.

Kurbegovic A., Cote O., Couillard M., Ward C.J., Harris P.C. & Trudel M. 2010. Pkd1 transgenic mice: adult model of polycystic kidney disease with extrarenal and renal phenotypes. *Hum Mol Genet* 19: 1174-1189.

Laiho A., Kotaja N., Gyenesei A. & Sironen A. 2013. Transcriptome profiling of the murine testis during the first wave of spermatogenesis. *PLoS One* 8: e61558. doi:10.1371/journal.pone.0061558.

Lechtreck K.F. 2015. IFT-Cargo Interactions and Protein Transport in Cilia. *Trends Biochem Sci* 40: 765-778.

Leenaars M. & Hendriksen C.F. 2005. Critical steps in the production of polyclonal and monoclonal antibodies: evaluation and recommendations. *ILAR J* 46: 269-279.

Lehti M.S. & Sironen A. 2016. Formation and function of the manchette and flagellum during spermatogenesis. *Reproduction* 151: R43-54.

Lehti M.S., Zhang F.P., Kotaja N. & Sironen A. 2017. SPEF2 functions in microtubule-mediated transport in elongating spermatids to ensure proper male germ cell differentiation. *Development* 144: 2683-2693.

Lehti M.S., Henriksson H., Rummukainen P., Wang F., Uusitalo-Kylmala L., Kiviranta R., Heino T.J., Kotaja N. & Sironen A. 2018. Cilia-related protein SPEF2 regulates osteoblast differentiation. *Sci Rep* 8(1): 859. doi:10.1038/s41598-018-19204-5.

L'Hernault S.W. & Rosenbaum J.L. 1983. Chlamydomonas alpha-tubulin is posttranslationally modified in the flagella during flagellar assembly. *J Cell Biol* 97: 258-263.

Liu W., Sha Y., Li Y., Mei L., Lin S., Huang X., Lu J., Ding L., Kong S. & Lu Z. 2019. Loss-of-function mutations in SPEF2 cause multiple morphological abnormalities of the sperm flagella (MMAF). *J Med Genet* 56: 678-684.

Mahmood T. & Yang P.C. 2012. Western blot: technique, theory, and trouble shooting. *N Am J Med Sci* 4: 429-434.

Malicki J. & Avidor-Reiss T. 2014. From the cytoplasm into the cilium: bon voyage. *Organogenesis* 10: 138-157.

Malicki J.J. & Johnson C.A. 2017. The Cilium: Cellular Antenna and Central Processing Unit. *Trends Cell Biol* 27: 126-140.

McAninch D., Mäkelä J.A., La H.M., Hughes J.N., Lovell-Badge R., Hobbs R.M. & Thomas P.Q. 2020. SOX3 promotes generation of committed spermatogonia in postnatal mouse testes. *Sci Rep* 10: 6751. doi:10.1038/s41598-020-63290-3.

Norris D.P. & Grimes D.T. 2012. Mouse models of ciliopathies: the state of the art. *Dis Model Mech* 5: 299-312.

Oh E.C. & Katsanis N. 2012. Cilia in vertebrate development and disease. *Development* 139: 443-448.

Olbrich H., Schmidts M., Werner C., Onoufriadis A., Loges N.T., Raidt J., Banki N.F., Shoemark A., Burgoyne T., Al Turki S., Hurles M.E., UK10K Consortium, Köhler G., Schroeder J., Nürnberg G., Nürnberg P., Chung E.M., Reinhardt R., Marthin J.K., Nielsen K.G., Mitchison H.M. & Omran H. 2012. Recessive HYDIN mutations cause primary ciliary dyskinesia without randomization of left-right body asymmetry. *Am J Hum Genet* 91: 672-684.

Ostrowski L.E., Andrews K., Potdar P., Matsuura H., Jetten A. & Nettesheim P. 1999. Cloning and characterization of KPL2, a novel gene induced during ciliogenesis of tracheal epithelial cells. *Am J Respir Cell Mol Biol* 20: 675-683.

Ostrowski L.E., Yin W., Rogers T.D., Busalacchi K.B., Chua M., O'Neal W.K. & Grubb B.R. 2010. Conditional deletion of dnaic1 in a murine model of primary ciliary dyskinesia causes chronic rhinosinusitis. *Am J Respir Cell Mol Biol* 43: 55-63.

Palchetti S., Pozzi D., Marchini C., Amici A., Andreani C., Bartolacci C., Digiacomo L., Gambini V., Cardarelli F., Di Rienzo C., Peruzzi G., Amenitsch H., Palermo R., Screpanti I. & Caracciolo G. 2017. Manipulation of lipoplex concentration at the cell surface boosts transfection efficiency in hard-to-transfect cells. *Nanomedicine* 13: 681-691.

Parisi M.A. 2019. The molecular genetics of Joubert syndrome and related ciliopathies: The challenges of genetic and phenotypic heterogeneity. *Transl Sci Rare Dis* 4: 25-49.

Pillai-Kastoori L., Heaton S., Shiflett S.D., Roberts A.C., Solache A. & Schutz-Geschwender A.R. 2020. Antibody validation for Western blot: By the user, for the user. *J Biol Chem* 295: 926-939.

Praveen K., Davis E.E. & Katsanis N. 2015. Unique among ciliopathies: primary ciliary dyskinesia, a motile cilia disorder. *F1000Prime Rep* 7: 36-36. doi:10.12703/P7-36.

Prevo B., Scholey J.M. & Peterman E.J.G. 2017. Intraflagellar transport: mechanisms of motor action, cooperation, and cargo delivery. *FEBS J* 284: 2905-2931.

Rayner R.E., Makena P., Prasad G.L. & Cormet-Boyaka E. 2019. Optimization of Normal Human Bronchial Epithelial (NHBE) Cell 3D Cultures for in vitro Lung Model Studies. *Sci Rep* 9: 500-018-36735-z, doi:10.1038/s41598-018-36735-z.

Reiter J.F. & Leroux M.R. 2017. Genes and molecular pathways underpinning ciliopathies. *Nat Rev Mol Cell Biol* 18: 533-547.

Roncaglia P., van Dam T.J.P., Christie K.R., Nacheva L., Toedt G., Huynen M.A., Huntley R.P., Gibson T.J. & Lomax J. 2017. The Gene Ontology of eukaryotic cilia and flagella. *Cilia* 6: 10. doi:10.1186/s13630-017-0054-8.

Rubbo B., Shoemark A., Jackson C.L., Hirst R., Thompson J., Hayes J., Frost E., Copeland F., Hogg C., O'Callaghan C., Reading I., Lucas J.S. & National PCD Service U. 2019. Accuracy of High-Speed Video Analysis toÂ Diagnose Primary Ciliary Dyskinesia. *Chest* 155: 1008-1017.

Sha Y., Liu W., Wei X., Zhu X., Luo X., Liang L. & Guo T. 2019. Biallelic mutations in Sperm flagellum 2 cause human multiple morphological abnormalities of the sperm flagella (MMAF) phenotype. *Clin Genet* 96: 385-393.

Silverman M.A. & Leroux M.R. 2009. Intraflagellar transport and the generation of dynamic, structurally and functionally diverse cilia. *Trends Cell Biol* 19: 306-316.

Sironen A., Uimari P., Iso-Touru T. & Vilkki J. 2012. L1 insertion within SPEF2 gene is associated with increased litter size in the Finnish Yorkshire population. *J Anim Breed Genet* 129: 92-97.

Sironen A., Vilkki J., Bendixen C. & Thomsen B. 2007. Infertile Finnish Yorkshire boars carry a full-length LINE-1 retrotransposon within the KPL2 gene. *Mol Genet Genomics* 278: 385-391.

Sironen A., Thomsen B., Andersson M., Ahola V. & Vilkki J. 2006. An intronic insertion in KPL2 results in aberrant splicing and causes the immotile short-tail sperm defect in the pig. *Proc Natl Acad Sci U S A* 103: 5006-5011.

Sironen A., Hansen J., Thomsen B., Andersson M., Vilkki J., Toppari J. & Kotaja N. 2010. Expression of SPEF2 during mouse spermatogenesis and identification of IFT20 as an interacting protein. *Biol Reprod* 82: 580-590.

Sironen A., Kotaja N., Mulhern H., Wyatt T.A., Sisson J.H., Pavlik J.A., Miiluniemi M., Fleming M.D. & Lee L. 2011. Loss of SPEF2 function in mice results in spermatogenesis defects and primary ciliary dyskinesia. *Biol Reprod* 85: 690-701.

Sorusch N., Yildirim A., Knapp B., Janson J., Fleck W., Scharf C. & Wolfrum U. 2019. SANS (USH1G) Molecularly Links the Human Usher Syndrome Protein Network to the Intraflagellar Transport Module by Direct Binding to IFT-B Proteins. *Front Cell Dev Biol* 7: 216. doi:10.3389/fcell.2019.00216.

Stillwell P.C., Wartchow E.P. & Sagel S.D. 2011. Primary Ciliary Dyskinesia in Children: A Review for Pediatricians, Allergists, and Pediatric Pulmonologists. *Pediatr Allergy Immunol Pulmonol* 24: 191-196.

Szymanska K. & Johnson C.A. 2012. The transition zone: an essential functional compartment of cilia. *Cilia* 1: 10. doi:10.1186/2046-2530-1-10.

Thermo Fisher Scientific Pierce BCA Protein Assay manual. 2020. (Accessed 10.11.2020). https://assets.thermofisher.com/TFS-Assets/LSG/manuals/MAN0011430_Pierce_BCA_Protein_Asy_UG.pdf.

Tran P.V., Haycraft C.J., Besschetnova T.Y., Turbe-Doan A., Stottmann R.W., Herron B.J., Chesebro A.L., Qiu H., Scherz P.J., Shah J.V., Yoder B.K. & Beier D.R. 2008. THM1 negatively modulates mouse sonic hedgehog signal transduction and affects retrograde intraflagellar transport in cilia. *Nat Genet* 40: 403-410.

Tsang W.Y. & Dynlacht B.D. 2013. CP110 and its network of partners coordinately regulate cilia assembly. *Cilia* 2: 9. doi:10.1186/2046-2530-2-9.

Tu C., Nie H., Meng L., Wang W., Li H., Yuan S., Cheng D., He W., Liu G., Du J., Gong F., Lu G., Lin G., Zhang Q. & Tan Y.Q. 2020. Novel mutations in SPEF2 causing different defects between flagella and cilia bridge: the phenotypic link between MMAF and PCD. *Hum Genet* 139: 257-271.

Uniprot database. Mouse SPEF2 domains. 2020. (Accessed 10.11.2020). Spef2 - Sperm flagellar protein 2 - Mus musculus (Mouse) - Spef2 gene & protein (uniprot.org)

Wheway G., Mitchison H.M. & Genomics England Research Consortium. 2019. Opportunities and Challenges for Molecular Understanding of Ciliopathies-The 100,000 Genomes Project. *Front Genet* 10: 127. doi:10.3389/fgene.2019.00127.

Xiao Z., Zhang S., Mahlios J., Zhou G., Magenheimer B.S., Guo D., Dallas S.L., Maser R., Calvet J.P., Bonewald L. & Quarles L.D. 2006. Cilia-like structures and polycystin-1 in osteoblasts/osteocytes and associated abnormalities in keletogenesis and Runx2 expression. *J Biol Chem* 281: 30884-30895.

Yuan X., Serra R.A. & Yang S. 2015. Function and regulation of primary cilia and intraflagellar transport proteins in the skeleton. *Ann N Y Acad Sci* 1335: 78-99.

Zhang H. & Mitchell D.R. 2004. Cpc1, a Chlamydomonas central pair protein with an adenylate kinase domain. *J Cell Sci* 117: 4179-4188.

APPENDIX 2. SPEF2 FRAGMENT FOR ANTIBODY PRODUCTION

Amino acids 550-850 of testis-specific isoform. Spef2 - Sperm flagellar protein 2 - Mus musculus (Mouse) - Spef2 gene & protein (uniprot.org)

```
       560        570        580        590        600
GKTPPTQEDD KRDPVVNQEK VSKTQDKNVL AVSPVPGDRT SQKEGVKINE
       610        620        630        640        650
FEQFRSSDSF LSLSMRAQLG AKSELMLRRG KSIPDILLVS ILVNAIKEIP
       660        670        680        690        700
VDQSWVLDGF PITLNQAKLL EEALTGYKRK FLQLKKKKEQ MPTLALDPST
       710        720        730        740        750
STEVSLLPSA LDFVILLDIS DNSSLARTND IIAKEISHEI SHENVGRPGT
       760        770        780        790        800
GTSQDNKSED RNLRDHIQHR IVGFLDNWPL LEEWFTQPKN ILTKVNAEID
       810        820        830        840        850
EALLCQKVKE IFATETVNKK IKVEKTLEEK ETEKKAGAPP AEPPAMSPPL
```

APPENDIX 2. SPEF2 TRANSFECTIONS, TESTIS-SPECIFIC DNA SEQUENCES

5´TE

TTCACCAGTGAGCTATGTCGGAAATCCTGTGCCAGTGGCTCAACCAGGAGTTGAGGGTGTC
CCGGACCGTGAGTCCCAAGTCATTTGCAAAGGCATTTTCTAATGGCTATCTAATTGGAGAA
GTTCTGTTCAAGTTTGAACTTCAGAGTGATTTTGCAGAATTTTCAGAGAGCAGGGGTTCAAC
AGCCAAGCTTAACAATTTCTCCCGCTTGCAACCAACACTTCACCTGCTGGGTTTGCAGTTTG
ATCAGAATGTGGCTCAAAGCATCATCACAGAGAAGCCTGGGGCAGCAACCAAACTTCTGT

ATCAGTTGTACATTGCTCTTCAGAAAAAGAAGAAAACAGGGCTGACTGGACTAGAGATAC
AAACCATGCAACCCCAGACAAACTTGAGGCTTCAGACCCTCAAAAGTGAGGCTTTTCGAG
AGAGACTTAAAAACCTGATACCACGGCAAACCGATTTCAATCTGATGCGGGTTACATGCA
GGTTTCAAGAAAAGTGTAAACAAATGAAAGAAGATCTTGCCCGAATGAATTTTGAGAAGT
TTGAAAAAATTCAAAAACTTGAGGAAGAGCAAAGACACTTTAATATCGAAAAGCAACGCT
TAAACAGAAGACGACAAAATGAGATAATGGCCAAAATCCAGGCAGCCATTATACAGATC
CCCAAGCCTGAATCCAACCGTACTTTGAAAGCTATTGAGGCTCAAAAACTGATGAAAAAG
AAAAAGGAGGCAGAGGACGTGGCCAATGAGATTAAGAAATTTGAAGCACTAATTAAAAA
GGATCTCCAAATTAAAGAAAGTGTATCCAAGACTTCTTTAGAAACAACAGACCAGACAAC
TGCAGAACTGCTCAACACTTATTCAGATGATGACTACATTAAAAAGATCCAGAAACGCCT
AGAAGAAGACGCTTTCGCACGCGAGCAAAGGGAAAAAAGACGACGCAGATTGTTGATGG
ATCAGCTAATGGCCCATGAAGCACAGGAGGAGGCCTATCGGGAAGAGCAGCTCATTCACC
GGCTCATGCGCCAGTCCCAGCAGGAGCGCAGGATTGCTGTGCAGCTCATGCATGTTCGCCA
CGAGAAGGAAGTTTTGTGGCAAAATAGAATTTTCCGAGAGAAACAATTTGAAGAAAGACG
ACTTAAGGATTTCCAGGATGCTCTTGATAGAGAAGCGGCTCTTGCCAAACAAGCCAAGATT
GATTTTGCAGAACAAACCTTGAGGGAGAAGGAAATTCATGAAAAGATCTCTGTGGAAAGA
GCCCAACAGCGTTATAAGAAGCATTATGGGATATGTGCAGAGATTTTGGATCAAATGCTA
GATTTGTGCACGAAGGTGGCAGACTATAGGTTGCTGACAAATAATCTTATTCCACATAAGA
TGATGCACGATTGGAAAGAACTGTTTTTTAGTGGAATTCCCATATATGAACAGACTTCTCTT
ACACATGGACAAACAGAACCCACTGAGGATCACCGTGCAGAAGTGAAGAAAAGGAACTT
ACTCGATAGCAAAGATTATGAAGATTATAAGAACATGGTTGGAGAGTGGG

KAD

TTGCGGTCAAGGGTTGTATACTGGGGAAGACACTCAGTGGAAAAACTACTGTTCTAAAGTC
TCTACAAAATGACTTTCCTGTTCATGTGCTTTCTATTGATACTCTTGTCCAAGAGGCTATCCA
GGCGTTTCATGAAAGACAAAAAAGCGGTAAGACACCACCAACTCAGGAAGATGATAAAA
GAGATCCTGTAGTGAACCAGGAAAAAGTGAGCAAAACTCAGGATAAAAATGTGTTAGCA
GTTAGTCCAGTTCCAGGGGACAGAACATCCCAAAAAGAAGGTGTCAAGATTAATGAATTT
GAACAGTTCAGATCAAGTGATAGCTTTTTATCACTTAGCATGCGAGCTCAACTTGGTGCAA
AGTCAGAGTTGATGCTTAGAAGAGGAAAGAGCATTCCAGACATACTTCTGGTCAGCATCCT
GGTAAATGCTATAAAGGAGATACCTGTGGACCAAAGCTGGGTTCTTGATGGATTTCCAATA
ACATTAAATCAAGCCAAACTCCTGGAGGAAGCACTTACAGGGTACAAAAGAAAATTCCTA
CAGTTAAAGAAGAAGAAAGAACAAATGCCCACATTGGCCCTAGACCCCTCAACTTCCACA
GAGGTCTCTCTTCTCCCATCTGCACTTGATTTTGTCATATTGCTAGATATTTCCGATAACTCA
TCGTTGGCTCGAACTAATGATATCATAGCTAAAGAAATCTCACATGAAATTTCTCATGAAA

ATGTTGGCCGTCCTGGAACTGGTACAAGCCAAGATAATAAGAGCGAGGACCGGAACTTAA
GAGACCACATACAGCACAGAATTGTTGGCTTCTTGGACAACTGGCCACTGTTGGAAGAGT
GGTTTACACAGCCAAAAAACATTCTGACGAAAGTCAATGCTGAAATAGATGAAGCGCTCT
TATGCCAAAAAGTAAAAGAAATTTTTGCTACTGAAACAGTAAACAAAAAGATCAAAGTTG
AAAAGACACTGGAAGAAAAGGAAACTGAGAAAAAGGCAGGAGCTCCCCCGGCTGAGCCT
CCCGCTATGAGCCCTCCCCTTTCTTCTGAAGCAGAAAAAGACAAGGAGCTTCATCAGGCA
AAAACTCCTGGGAAAGGAAAGACACAATCAGTTTCTCCTAAAGGAAAAGCACAAGGAGG
CAAAGTTTCAGTAAAGAAATCACCGGTTGGCTCAGCAGAAGTATCACCCACACCAACAGC
ACCACCGCCACCTAAGGCAGGAACAGAAGAATGGGTTTATGTGAATGAGCCTATACCGGA
GGAACTCCCTTCATTTTTGGTACCTTACTGGGAACTGATAGAGAAATCCTACATCAACCAC
ATCAAAACAGTACTTCGACATCTCAGAGAGAGACAGCACAATGTGCTCTCTTATTTATATG
AGACTAGGACAAGTTTCCAGGAGTTTCTACGGCGTCCAGATCACAAGCAAGATTTTGTATC
TCAGTGGCAGGCTGATTTCAACTCTGTTCCTGAAGACCTGTGGGAAGATGAGGAAACAAA
GGCTGAGCTACACCAAAGAGTAAATGATCTGCGAGACCGCCTATGGGACATCTGTGAAGC
GAGGAAGGAAGAGGCGGAACAGGAGAGGCTTGATATCATTAATGAGAGCTGGCTGCAGG
ACTCTATCGGAATCACAATGAATCATTTCTTTTCCCTGATGCAGGCAGAAGTGAACCGTTTT
CAAGATACCAAAAGACTCCTTCAAGATTATTACAGAGCAATGGAATCCAAAATCCCTCTG
GAAGACAGTAAGAAATTTACTCGGGTCCCATTGGTTCAGCTTGATGGTAAAGAAATTTCAG
AAAGCCAGCTCAGAATTCCTCTAGTTCCTCGAATATCCAATTCTCCAGAAAATTCTGCCGT
CAAGCCAAAGGTGGGGACATTTCTGAAGGGC:AGATCTGAT:CCTCCTTTAGAAGTCCTGGA
AGCCAACTTTGAAATAGATGAGAAGATTTTATTGGACACCTGGCAGCAGGCTTCATTAGCC
ATCTCTAACATGGTGGCTGCTGAAGTTCACCAAAGGCTCACAGAGGAAGAAAAAGAACCA
CCCCAATTAGATTCCAAAGAAAAGTCTCCTCAGTCAGGTGCAAATAAAAAAGCCAAGAAG
GAGAAAGAAGCACCCAAGAAGAAAAAGACAGACAAGAAAGGAAAAGGTATTCACGGCA
CTAGGACCTGGTCCACAGGCAAATCATCCCCCGTGGCAGAAGTCAGTCCAGTCACAGTCA
CACCTGAGGAAATGGCTGAGATGGAAAAGAGGA

3´TE

AACAAGCCGCACAATTTCGACTTGAGCTAATAAAGTTGAAAGCTTTGTCCGTCCTGGAAGA
TTTAGTAACAAAGGTGATTGATGTCTACAGGCTCATGGAAAAATGGCTTGGTAAGAGATAT
TTGAATGAAATGGCCAGTATACAGAAATTGACCGAATTAGCTCGCTACCACATTGAAACA
GCTACAAAAATTCAAAATGAGATTTACTTAAGCCAAGAAGACTTCTATATCAATGGAGAC
ATAAAAGTCTTCCCAGATCCTTCTCCACCAACCCGCCCACCACCAGTAGAAAGGGAAGAA
AATGGTACCCTAACAATCGAACAGCTTGATAATCTTCGAGATCAGTTCTTAGACATGGCAC
CTAAAGGCATAATCGGAAATAAAGCCTTCAGTGACATTCTGCTTGATTTGATTACCCTAAA

CCTTGGAACCAATAACTTCCCTAGCAGCTGGATGCACCTCAGCCAACTGGACTTGCAGGA
GATCACATCTTTATTAACAGTCAACACAGAGTTCGTGGACTGGAGGAAGTTCTTGATGGTC
ACAGCCATGCCGTGGCCCATGGCCCTGGAGGATGAGCTTCTGGACACCCTGCAGAGGTTT
AAGGCCCTGGATGAAGCACAGACAGGCACCATCACCTACGAACAGTATAAGCAGGCTGG
TCTATGGTTTTCAGGAGATGAAGATATAAAAATTCCAGAAAATCCCCTTGAACCCTTGCCA
TTCAATCGACAGGAGCATCTTATAGAGTTCTTCTTTAGGCTGTTTGCGGACTGTGAGAAGG
AGCCACCTCAGCTTGACTACACTCAGATGCTGCTGTATTTTGCGTGCCACCCAGACACTTTG
GAAGGAGTCTACAGGGCCCTCAGTGTGGCTGTGGGAACTCACATCTTCCGCCAGGTTGAA
ACTCCGATGCTGATGGCAGAAAAGACCTCCATCTCCACTGTGAGTCCCATTGAGGAATTCC
CTGAGACTGAGGAAAGTAGTGCAAAAGAGGACCGGGAACTGAAGGAGGAGAAAGATGA
CCAAAAGGAAGAAGAAATTCCCGAAAATGCAAACACTGAAAAGATTTCCATGGAAACAC
TGCTCAAAGTGTTTGGAGGAGGAAATGAAGTACTGGATGCCAACAGATTTGCCAGCTACC
TAAAATCAGAGAATATTTATGCAGAGAATTTCATCAAGACTTTTCAGGACCTGGGTGCCAG
GAACCTGGAGCCAATTGCAGTTAATATTCTCTTGAAGCATCCTTACATTCAGGACCTGATT
GCAAATTATGTAGACTATAAATTTCCTGACATTAAAATGATTCTTCAAAGGAGTGAGCATG
CACAAGGCAGTGATGGAGAAAGGTCACCCTCAAGACTTACAGACGAAAAGA